iScience

Article

# Highly immunogenic DNA/LION nanocarrier vaccine potently activates lymph nodes inducing long-lasting immunity in macaques

## Graphical abstract

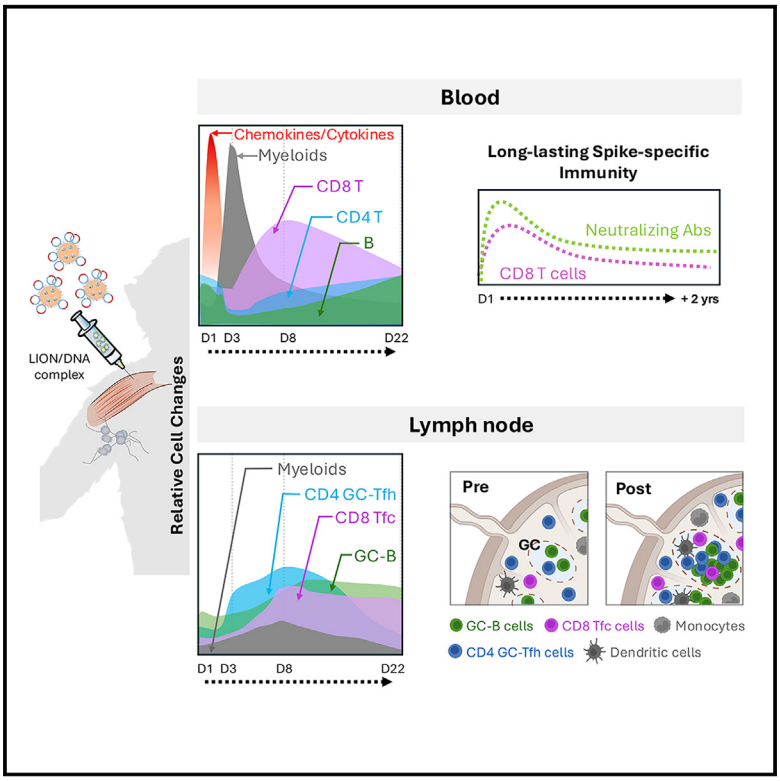


## Highlights

- DNA/LION vaccine induces robust and durable immune responses in macaques
- Simple formulation induces strong neutralizing antibody and cellular immunity
- DNA/LION vaccine activates lymph nodes and expands germinal centers
- Cytokine responses correlate with myeloid and lymphoid cell changes in blood and LN

## Authors

Sevasti Karaliota, Maha Moussa, Margherita Rosati, ..., Steven G. Reed, George N. Pavlakis, Barbara K. Felber

## Correspondence

barbara.felber@nih.gov

## In brief

Natural sciences; Biological sciences; Immunology; Immune response; Biotechnology; Nanotechnology

Karaliota et al., 2025, iScience *28*, 112232
April 18, 2025 Published by Elsevier Inc.
https://doi.org/10.1016/j.isci.2025.112232

CellPress

iScience

CellPress
OPEN ACCESS

Article

# Highly immunogenic DNA/LION nanocarrier vaccine potently activates lymph nodes inducing long-lasting immunity in macaques

Sevasti Karaliota,[1,2,8] Maha Moussa,[1,8] Margherita Rosati,[1] Santhi Devasundaram,[1] Soumya Sengupta,[1] Katherine C. Goldfarbmuren,[3,4] Robert Burns,[1] Jenifer Bear,[1] Dimitris Stellas,[1] Elizabeth A. Urban,[5] Claire Deleage,[5] Amit P. Khandhar,[6] Jesse Erasmus,[6] Peter Berglund,[6] Steven G. Reed,[6] George N. Pavlakis,[7] and Barbara K. Felber[1,9,*]

[1]Human Retrovirus Pathogenesis Section, Vaccine Branch, Center for Cancer Research, National Cancer Institute, Frederick, MD, USA
[2]Basic Science Program, Leidos Biomedical Research, Inc., Frederick, MD, USA
[3]Advanced Biomedical Computational Science, Leidos Biomedical Research, Inc., Frederick, MD, USA
[4]Vaccine Branch, Center for Cancer Research, National Cancer Institute, Bethesda, MD, USA
[5]AIDS and Cancer Virus Program, Frederick National Laboratory for Cancer Research, Frederick, MD, USA
[6]HDT Bio Corp, Seattle, WA, USA
[7]Center for Cancer Research, National Cancer Institute, Frederick, MD, USA
[8]These authors contributed equally
[9]Lead contact
*Correspondence: barbara.felber@nih.gov
https://doi.org/10.1016/j.isci.2025.112232

## SUMMARY

A SARS-CoV-2 spike DNA vaccine formulated with a cationic nanoparticle emulsion (LION) was tested in Rhesus macaques. It induced robust, long-lasting (>2 years) cellular and humoral immunity, including increased neutralization breadth. T cell responses were predominantly $CD8^+$, in contrast to other DNA vaccines. A rapid transient cytokine/chemokine response was associated with expansion and trafficking of myeloid cells and lymphocytes. Increased proliferation and dynamic changes between blood and lymph node (LN) were found for monocyte-derived cells, dendritic cells, and B and T cells, resulting in activation of LN and expansion of germinal centers (GCs), likely critical in shaping long-lasting adaptive immunity. Significant GC expansion of B, CD4−, and CD8− cells, including the Tfc3 subset, reflects a balanced immune response, including antibody (Ab) development. DNA/LION vaccination activates myeloid and lymphoid cells in blood and LN and promotes effective antigen presentation, resulting in sustained antigen-specific cellular and humoral responses, emerging as an effective DNA vaccine delivery platform.

## INTRODUCTION

The successful response to the recent SARS-CoV-2 pandemic demonstrated the power of a rapidly deployable, cost-effective and simple vaccine. Nucleic acid-based vaccines have several important advantages over other vaccine regimens that are based on viral vectors and proteins, including simplicity of vaccine design and rapid implementation with predictable scale-up production. Nucleic acid-based vaccines can be administered repeatedly without concern about anti-vector immunity.[1–9] DNA, mRNA or alphavirus-derived self-amplifying replicon (rep) RNA vaccines are delivered by intramuscular (IM) or intradermal injection. Naked DNA uptake is enhanced by *in vivo* electroporation (EP) resulting in higher immunogen expression and increased immunogenicity. Inclusion of cytokine DNA producing interleukin (IL)-12 was shown to significantly increase HIV immune responses in macaques and humans.[10–14] DNA vaccination induces durable immune responses in macaques.[15–20] mRNA vaccines require formulation with lipid nanoparticles (LNPs)[2,4] and are inducing protective immunity against SARS-CoV-2 in humans.[21–24] RepRNA, complexed with the cationic nanocarrier Lipid InOrganic Nanoparticle (LION), was also shown to induce robust immune responses in animal models[25–30] and humans.[31]

In this report, we evaluated the LION formulation for delivery of a DNA vaccine. In contrast to LNP formulations, the nucleic acid is attached to the cationic surface of LION nanocarriers, which serves as vehicle to protect and deliver the cargo efficiently into the muscle cells[25] whereas LNPs encapsulate the cargo inside the nanoparticle. LION is a refrigerator-stable formulation that is easy to use by performing a simple admixture step with the nucleic acid payload before IM injection. Here, we tested the DNA/LION vaccine platform for its ability to induce innate and adaptive immune responses in rhesus macaques using SARS-CoV-2 spike DNA as a model. We demonstrated that DNA/LION vaccination induced both robust and long-lasting (>2 years) cellular and humoral responses. Our data showed rapid coordinated and transient (4–24 h) cytokine/chemokine

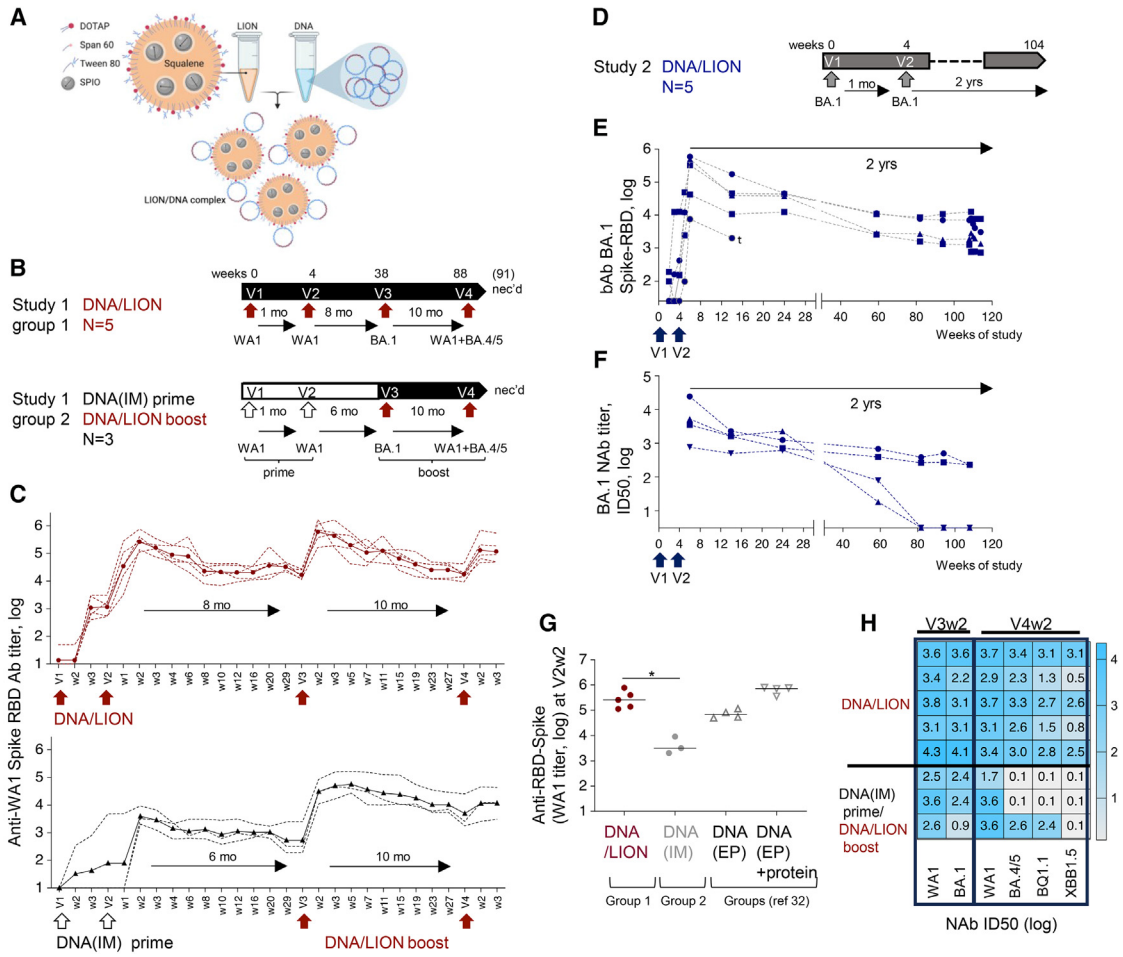


**Figure 1. DNA/LION vaccine induces durable antibody responses in rhesus macaques**

(A) Schematic representation of DNA/LION vaccine. The supercoiled plasmid DNA is depicted as circles. Cartoon is modified from Erasmus et al.[21]

(B) Schematic representation of DNA vaccine administration in study 1. Group 1 ($n = 5$) received 4 vaccinations (V1–V4) with the indicated spike DNA/LION via intramuscular (IM) injection. Group 2 ($n = 3$) received 2 priming vaccinations with naked spike DNA via IM route (DNA(IM)), followed by 2 booster vaccinations with spike DNA/LION. The animals were necropsied at week 91.

(C) Anti-WA1 spike-RBD Abs were measured by ELISA. Median values are shown with dots.

(D) Schematic representation of DNA/LION vaccination in study 2. Macaques ($n = 5$) were vaccinated twice (V1, V2; week 0 and 4) with BA.1 spike DNA/LION via IM and were monitored for 2 years.

(E and F) In study 2, anti-BA.1 spike-RBD Ab and NAb were measured longitudinally. MC74 developed health issues 11 months after vaccination 2, evaluated as non-intervention-related, and the animal was sacrificed (t).

(G) Anti-WA1 spike-RBD Ab responses at 2 weeks after the 2$^{nd}$ vaccination (V2w2) induced by DNA/LION (study 1, group 1; $n = 5$) and DNA(IM) prime-DNA/LION boost (study 1, group 2; $n = 3$) compared to a historical study[32] examining spike DNA vaccination by electroporation (EP) alone ($n = 4$) or co-immunized with EM-005 adjuvanted spike protein ($n = 4$). Bars indicated median values. The $p$ values were calculated by Mann-Whitney Wilcoxon test and are defined as $\leq 0.05$, *.

(H) Magnitude and breadth of anti-spike NAb at 2 weeks after V3 and V4.

responses to the DNA/LION vaccine that associated with expansion and migration of different myeloid and lymphocyte cell subsets. We report significant expansions of GC-B cells, CD4 T follicular helper (Tfh), CD4 GC-Tfh, CD8 T follicular cells (Tfc1; CXCR5$^{+}$PD-1$^{int/high}$), including a subset of CXCR5$^{+}$ PD-1$^{high}$ Bcl-6$^{-/+}$ Tfc3 cells, reflecting cell subsets necessary for a balanced immune response including Ab development. Together, these data highlight the significant role of innate responses to vaccination by shaping the cellular and humoral adaptive immunity.

## RESULTS

### DNA/LION vaccine induces long-lasting antibody responses in macaques

The vaccine studied in this report comprises supercoiled DNA complexed with LION (Figure 1A). The LION nanocarrier composition is detailed elsewhere[27,28] and the oil phase contains squalene, 1,2-dioleoyl-3-trimethylammonium propane cationic lipid (DOTAP), sorbitan ester (SPAN 60), polyoxyethylene-80-sorbitan monooleate (Tween 80). LION is a refrigerator-stable, cationic

oil-in-water nanoparticle emulsion formulation with a 60 nm average hydrodynamic diameter.[33] Formulation of the nucleic acid payload is performed by a simple admixture step with LION before IM injection. LION-formulated nucleic acids exhibit distinct safety and biodistribution profiles compared to LNP formulations.[25,31]

Five Indian rhesus macaques (Table S1; study 1, group 1) were vaccinated with 2 mg DNA complexed with the LION formulation.[27,28] The vaccine was administered by IM injection for a total of 4 vaccinations (V1–V4) (Figure 1B, top panel). The sequential vaccinations used DNA vectors expressing 2P-stabilized ancestral SARS-CoV-2 WA1 spike (for V1, V2), BA.1 spike (for V3) and the bivalent WA1 and BA.4/5 spike combination (for V4).

Complete blood count/blood chemistry (CBC/Chem) analysis showed transient changes, which returned to baseline by day 8–15 (Figure S1). White Blood Cells transiently and rapidly increased, followed by lymphocytes (Figure S1A). Some enzymes also showed transient elevation (Figure S1B).

Humoral immune responses against WA1 spike receptor binding domain (spike-RBD) were measured after each vaccination and monitored over time (Figure 1C). Binding antibody (Ab) responses were detected in all DNA/LION vaccinated animals as early as 3 weeks after the 1$^{st}$ vaccination (V1w3) and increased upon the subsequent vaccinations, reaching maximal levels after the 2$^{nd}$ vaccination. After an initial contraction, Ab responses were maintained with a slow decay rate over the 8 and 10 months of follow-up after the 2$^{nd}$ and 3$^{rd}$ DNA/LION vaccination, respectively, demonstrating durability. To address Ab durability further, another group of 5 macaques (Table S1, study 2), which received 2 vaccinations with stabilized spike BA.1 DNA/LION, was also monitored (Figure 1D). Anti-spike BA.1-RBD Ab were still detected (median titer of 3.5 log) in all animals at 2 years after the 2$^{nd}$ vaccination (Figure 1E) and neutralizing Ab (NAb) were detected in all animals at 1 year, and in 2 of 4 animals for >2 years (Figure 1F). Together, these data showed strong durability of the spike DNA/LION-induced humoral immune responses.

To test the contribution of LION in the efficacy of the DNA/LION regimen, the responses in group 1 ($n$ = 5; study 1, group 1) were compared to responses obtained in macaques ($n$ = 3; study 1, group 2; Table S1), which received 2 priming vaccinations (V1, V2) with naked DNA without LION [DNA(IM)] (Figure 1B**, bottom panel**). The vaccine included the same dose of the same WA1 spike DNA administered directly by the IM route. DNA(IM) vaccination induced weaker and slower responses, with 1 of 3 animals scoring positive after V1, and ∼2 log lower Ab levels, which remained after V2, compared to levels obtained with DNA/LION (Figure 1C**, bottom panel**). The DNA(IM) primed group received subsequently 2 DNA/LION booster vaccinations (V3, V4), which increased Ab magnitude to levels similar as those of the DNA/LION group.

We further compared the humoral immune responses upon DNA/LION vaccination to responses obtained using other DNA delivery methods to rank the vaccine platforms. The Ab data were compared to historical data[32] obtained from macaques vaccinated with the same spike DNA delivered by EP either alone or co-immunized with Toll-like receptor 4 agonist glucopyranosyl liped adjuvant-stable emulsion (GLA-SE)-adjuvanted WA1 spike-RBD Protein (Figure 1G), reported in Rosati et al.[32] and were analyzed together with the current study samples. Comparison of the four different regimens after the 2$^{nd}$ vaccination (V2w2, when data were available for all groups) showed that the Ab magnitude induced by DNA/LION vaccine was similar those induced by regimens of DNA(EP) or DNA(EP)+adjuvanted spike protein co-immunization,[32] a regimen known to maximize Ab responses in macaques,[16,34,35] but was significantly higher than the levels obtained by unformulated DNA(IM) vaccination.

Anti-spike-specific neutralizing (NAb) responses were examined for their magnitude and breadth after V3 and V4. Similar NAb titers were found against WA1 and the closely related BA.1 spike pseudotyped viruses (Figure 1H). Interestingly, although the magnitude against WA1 was comparable at V4wk2, animals (study 1, group 1), which received 4 DNA/LION vaccinations showed better neutralization breadth against BA4/5, BQ1.1, XBB1.5 spike-carrying pseudotyped viruses, than animals primed with DNA(IM) and boosted with DNA/LION (study 1, group 2). Thus, despite similar WA1 Ab and NAb levels at V4w2, DNA/LION vaccinations induced broader NAb responses, including BQ1.1 and XBB1.5, compared to the DNA(IM) primed macaques indicating a benefit of stronger priming by DNA/LION. Of note, such NAb levels were shown to be protective in our previous SARS-CoV-2 challenge study.[32] Therefore, DNA/LION vaccination induced potent and durable binding and neutralizing Ab responses.

## DNA/LION vaccine induces long-lasting cellular responses in rhesus macaques

The DNA/LION vaccination also induced robust cellular spike-specific T cell responses (Figure 2A, upper panel) reaching up to 2% of circulating T cells measured by intracellular cytokine staining. These responses were also durable over the 8- and 10-month follow-up upon V2 and V3, respectively. In contrast, DNA(IM) vaccination induced lower responses, which lacked durability (Figure 2A, lower panel). Upon DNA/LION boosting (V3, V4) of the DNA(IM) animals (group 2), these responses were increased, reaching similar levels as the DNA/LION vaccinated animals (group 1). Similar robust cytokine$^+$ T cell responses were induced by animals in study 2 (Figure 2B). Analysis of the cytokine$^+$ T cells showed that they were mainly interferon (IFN)-γ single-positive (∼77%), ∼15% IFN-γ/tumor necrosis factor (TNF)-α double-positive and a minority (∼8%) TNF-α single-positive, similar to DNA/EP vaccine responses[36] (Figure 2B, right panel). Monitoring durability of these cellular responses over longer time (Figure 2B) showed that antigen-specific T cells were still detectable at 2 years post V2 with median 0.03% (range 0.13–0.61) of circulating T cells. Thus, DNA/LION induced both long-lasting humoral and cellular immune responses.

Interestingly, DNA/LION induced a strong skewing toward CD8$^+$ T cell responses (Figure 2C). In contrast, priming by DNA(IM) or with DNA(EP) resulted in higher spike-specific CD4$^+$ T cells (V2w2; Figure 2C, upper panels). Similar results were reported prior[32] upon DNA(EP) vaccination (Figure 2C, upper and lower right panels), analyzed using the same gating strategy and FlowJo software. Boosting of the DNA(IM) primed animals with DNA/LION led to a substantial increase of spike-specific CD8$^+$ T cells (V3w2; Figure 2C, lower panels). We further

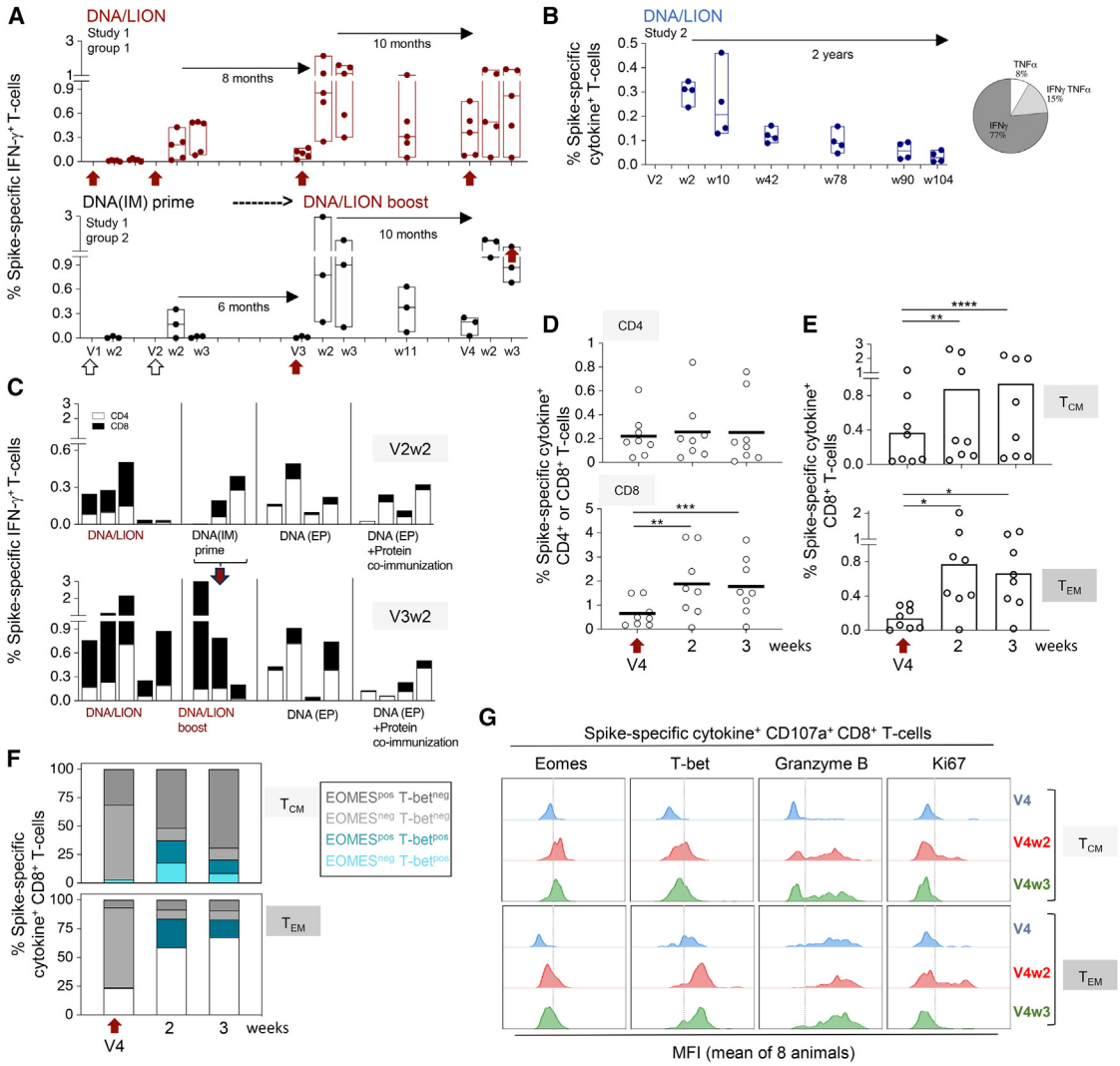


**Figure 2. DNA/LION vaccine induces durable T cell responses in rhesus macaques**

(A and B) Spike-specific T cell responses were measured in PBMCs over time by flow cytometry in (A) study 1, as IFN-$\gamma^+$ T cells, and (B) study 2, as cytokine$^+$ (IFN-$\gamma$, TNF-$\alpha$ single- and/or double-positive) T cells. Scatterplots with median line and minimum and maximum values are shown. The pie chart depicts the frequency of spike-specific IFN-$\gamma$, TNF-$\alpha$ single- and/or double-positive T cells.

(C) Comparison of CD4$^+$ and CD8$^+$ IFN-$\gamma^+$ spike-specific T cell responses induced by DNA/LION (study 1, group 1) and by DNA(IM) prime followed by DNA/LION boost (study 1, group 2) and a historical study[32] examining spike DNA vaccination by EP alone ($n$ = 4) or co-immunized with adjuvanted spike protein ($n$ = 4).

(D) Frequency of spike-specific cytokine$^+$ T cells CD4$^+$ and CD8$^+$ T cells at the day of V4 and 2 and 3 weeks later (study 1). Bars indicate mean values. $p$ values from generalized estimating equation (GEE) and are defined as $\leq$0.05, *; $\leq$0.01, **; $\leq$0.001, ***; $\leq$0.0001,****.

(E) Frequency of cytokine$^+$ spike-specific CD8$^+$ $T_{CM}$ (CD28$^+$ CD95$^+$) and $T_{EM}$ (CD28$^-$ CD95$^+$ CCR7$^-$) after V4. Scatterplots with mean values are shown.

(F) Proportion of cytokine$^+$ CD8$^+$ T cells expressing EOMES and/or T-bet (mean of 8 animals).

(G) Manually gated spike-specific cytokine$^+$ CD107a$^+$ CD8$^+$ $T_{CM}$ and $T_{EM}$ cells (V4 [blue], V4w2 [red], V4w3 [green]) were overlaid in histograms depicting expression of EOMES, T-bet, GzmB, and Ki67 (mean fluorescent intensity [MFI] as mean of 8 animals at each time point). Gray dotted line marks the border between the negative and positive population.

noted that the overall frequency of spike-specific CD4$^+$ T cells upon DNA/LION vaccination remained stable upon V4 (Figure 2D, upper panel), whereas the frequencies of CD8$^+$ T cells were significantly increased (Figure 2D, lower panel). These data demonstrated the strong CD8$^+$ T cell response mediated by DNA/LION vaccination, which was further boosted in subsequent vaccinations.

DNA/LION vaccination also significantly increased the frequencies of spike-specific CD8$^+$ memory responses, including both central ($T_{CM}$) and effector ($T_{EM}$) memory cells (Figure 2E, analysis after V4). T-bet and Eomesodermin (EOMES) are key transcription factors associated with effector function and memory T cell formation,[37,38] respectively. Importantly, these $T_{EM}$ cells expressed higher T-bet, a transcriptional factor supporting

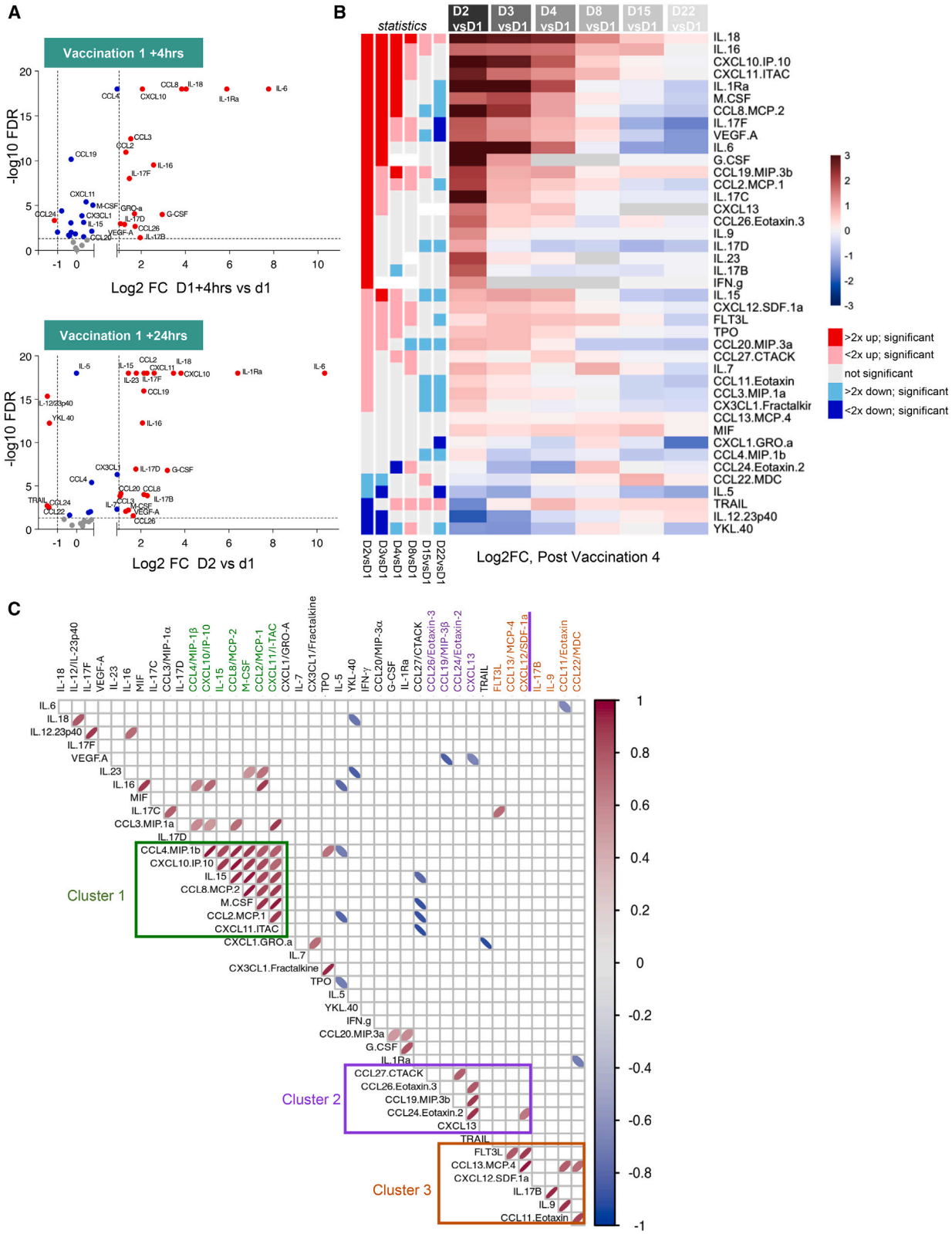


*(legend on next page)*

their expansion, differentiation and maturation toward a cytotoxic differentiation state[39] (Figure 2F). The spike-specific cytokine$^+$ (IFN-$\gamma$ and/or TNF-$\alpha$) CD107a$^+$CD8$^+$ T cells, including $T_{CM}$ and T-bet$^+$$T_{EM}$ fractions, displayed additional cytotoxic properties granzyme B (GzmB$^+$) and proliferative capabilities (Ki67$^+$) (Figure 2G), underscoring their potent activation levels and cytotoxic potential. Expression of all markers was sustained to week 3, except the proliferation marker Ki67, which was reduced, as expected. Together, these results demonstrated that the DNA/LION vaccine is a potent inducer of durable humoral and cellular immunity including induction of both potent NAb and multifunctional CD8$^+$ memory T cells with cytotoxic potential.

## DNA/LION vaccination induces rapid transient chemokine/cytokine changes in plasma

To explore the effect of the DNA/LION vaccination on induction of chemokine and cytokine responses, we performed a plasma proteomics analysis measuring their levels by multiplex immunoassays and ELISA. Of the 63-analytes panel, 41 analytes (Table S2) showed changes, displaying a similar pattern (Figure S2A) and similar magnitude after each vaccination (V1–V4) (Figure S2B). Interestingly, several analytes showed a significant early activation (+4 h) (Figure 3A, upper panel) depicted in the volcano plot, exemplified by IL-6, IL-18, IL-1Ra, CXCL10, CCL8. The responses were enriched by additional analytes, including IL-15, CCL2, CCL19, CXCL11, IL-23 at 24 h (D2) (Figure 3A, lower panel). Figure 3A highlights the innate responses immediately following the first encounter with the vaccine. Comparable responses were detected upon additional vaccinations (Figure S2). Detailed analysis of analyte changes over time (D2 to D22 compared to D1) upon V4 is depicted in a heatmap (Figure 3B). Similar patterns were observed upon vaccinations 1–3 (Figures S2A and S2B). Most of these increases were dimmed by D3/D4, returning to baseline by D8 to D15, as shown in the alluvial display (Figure S2C).

Among the increased analytes (Figures 3B, S2A, and S2B), we found several chemokines/cytokines produced by myeloid cells,[40,41] including CCL2/MCP-1, CCL19/MIP-3$\beta$, IL-6; IL-15, an activation and differentiation factor for multiple lymphocyte populations; the IFN-induced CXCL11/I-TAC and CXCL10/IP-10 coordinating the trafficking of T cells, natural killer (NK) and natural killer T (NKT) cells toward inflammatory sites[42]; as well as the proinflammatory IL-18 and the anti-inflammatory IL-1Ra, a regulator of the IL-1 pathway, reflecting vaccine-induced inflammation.[43,44] We also noticed significant changes in analytes associated with LN and germinal center (GC) activation including CXCL13, FLT3L and IL-7. FLT3L and IL-6[45–48] are also involved in the development of dendritic cell (DC) and B cells.[49,50] The combination of DNA/LION-induced plasma cytokine/chemokines were unique to this regimen. In contrast, only few and low changes were found upon DNA(IM) vaccination (Figure S3). These data further support the observation of a strong adjuvant effect by LION.

Evaluating the inter-relationship among analyte changes (Log2FC, D2 vs. D1), we identified a clusters of cytokine/chemokines showing concerted significant increases (Figure 3C), with a cluster (cluster 1, green box) comprising IL-15, CXCL10/IP-10, CCL2/MCP-1, CCL3/MIP-1$\alpha$, CCL8/MCP-2, M-CSF, CCL4/MIP-1$\beta$, CXCL11/I-TAC and two smaller ones including a cluster (cluster 2, purple box) comprising CXCL13, CCL24/Eotaxin-2, CCL26/Eotaxin-3, CCL19/MIP3$\beta$ and a cluster (cluster 3, brown box) comprising FLT3L, CCL13/MCP-4, CXCL12/SDF-1a, CCL11/Eotaxin, CCL22/MDC. We previously reported that several analytes in cluster 1, including IL-15, were part of a signature associated with enhanced humoral immune responses in Pfizer/BioNTech BNT162b2 mRNA vaccinated persons.[51–53] Analytes in clusters 2 and 3 are associated with LN activation.[45,47] Thus, our cytokine/chemokine analysis support the conclusion that the DNA/LION-induced unique and strong immune activation can contribute to the development of robust vaccine-induced adaptive immune responses.

## Dynamic redistribution of immune cells in LN and blood upon DNA/LION vaccination

To understand the nature of different cell subsets affected by DNA/LION vaccination, an extensive flow cytometric phenotyping analysis was performed. Peripheral blood mononuclear cells (PBMC) and lymph node mononuclear cells (LNMCs) were collected sequentially upon V4 (Figure 1A), including at the day of vaccination D1, D3 or D4 (referred to as combined D3/4 with $n$ = 4 macaques on each day), D8 and D22, at which time point the animals were necropsied. Myeloid and lymphocyte cell subsets were analyzed by immune phenotyping in blood and LN using multiparametric flow cytometry and high-plex spatial biology analysis (Figures 4, 5, 6, 7, and 8).

Both unsupervised clustering t-Distributed Stochastic Neighbor Embedding (t-SNE) and conventional gating strategies were employed. The t-SNE map clusters (Figure 4B) illustrate the baseline distribution (D1) of the cell populations among live cells in blood and lymph nodes (LNs), including HLA-DR$^{pos}$Lin$^{neg}$, T, and B cells, the focus of this work. Manual gating showed the dynamic

**Figure 3. Plasma cytokines/chemokines induced by DNA/LION vaccination**

Plasma proteomics was performed on samples collected upon vaccinations and analyzed for cytokines/chemokines by a chemiluminescent assay (Meso Scale Discovery, 61 plex) and ELISA for CXCL13.

(A) Volcano plots representation of Log2FC enrichment of analytes at 4 and 24 h after V1, respectively. Significantly changed ($p < 0.05$ by GEE, >2-fold; red dots; <2-fold, blue dots) analytes are shown. $p$ values < 1e−18 were set to 1e−18 for plotting −log10 of $p$ value.

(B) Heatmap shows cytokines/chemokine changes from 8 animals as Log2FC estimate from GEE in relation to the day of vaccination V4 (D1), including D2, D3, D4, D8, D15, and D22. $p$ values from GEE are summarized in the left columns with significant increase (red) and decrease (blue) with >2x and <2x upregulation are shown in respective shades. Gray bars indicate not analyzed analytes.

(C) Inter-relationship of the vaccine-induced effects on different analytes. Pairwise Spearman correlations were calculated between the log2FC at one day (D2) after the V4 vs. D1 for all biomarkers shown in (B). Significant correlations ($p$ value < 0.05) are represented by ellipses with color and shape corresponding to the value of the Spearman correlation coefficient with red color indicating a positive correlation. Three clusters of analytes with positive associations among Log2FC are denoted with boxes and lettering in green (cluster 1), purple (cluster 2), and brown (cluster 3).

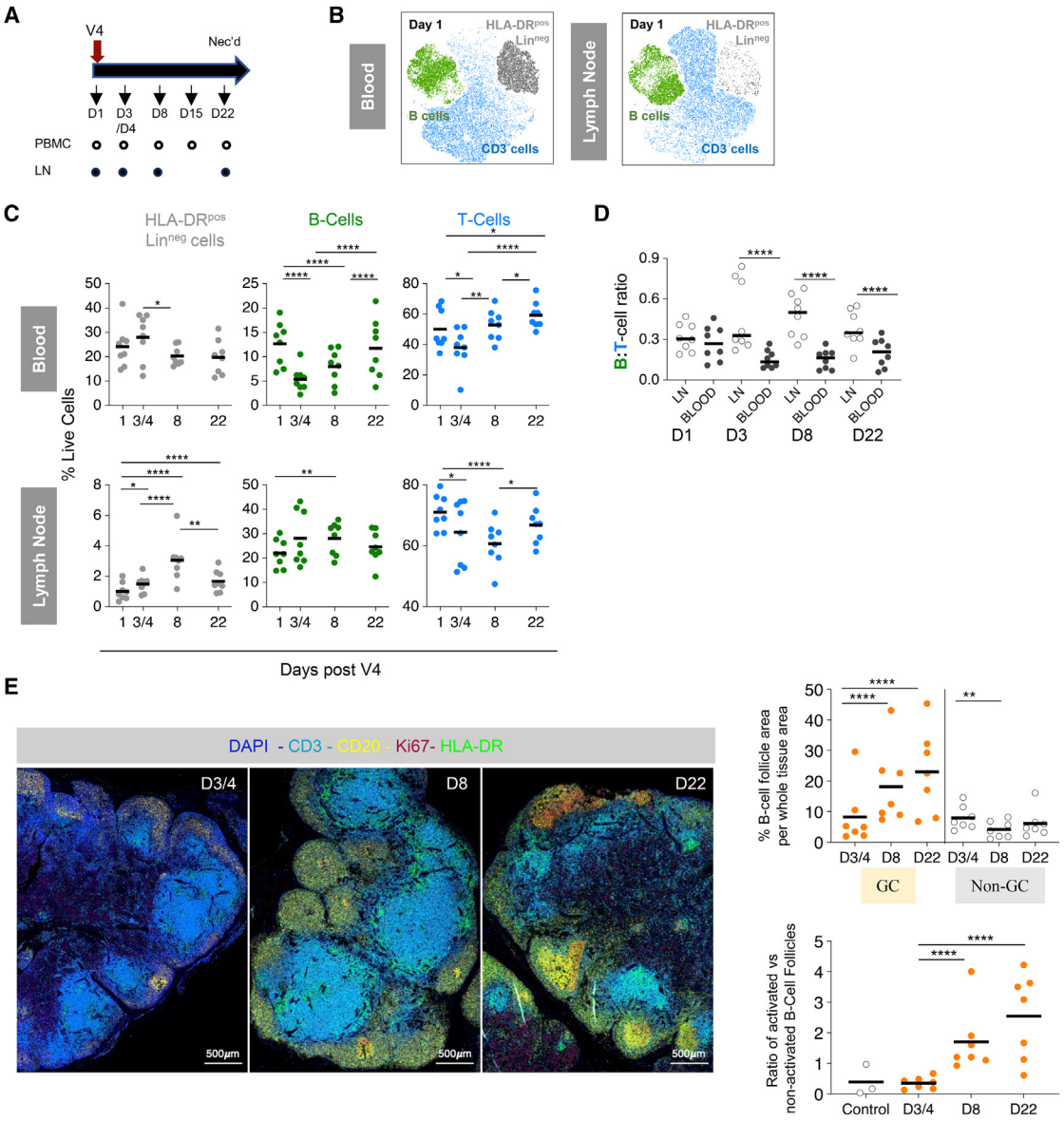


**Figure 4. Dynamic distribution of lymphocytes and myeloid cells in blood and LN upon DNA/LION vaccination**

(A) Cartoon outlining the blood and LN collection after V4.

(B) t-SNE analysis showing phenotypic clustering of equal numbers of blood and LN live cells on the day of the V4 (D1). Manually gated lineage subsets were overlayed on the t-SNE map and allocated a unique color (CD20$^+$ B cells [green], CD3$^+$ T cells [blue], and Lin$^{neg}$ HLA-DR$^{pos}$ cells [gray]).

(C) Manually gated cell subsets expressed as frequency of live cells. Bars indicate mean values. *p* values from GEE, 1, day of vaccination. The *p* values are defined as ≤0.05, *; ≤0.01, **; ≤0.001, ***; ≤0.0001,****.

(D) B-to-T cell ratio in blood and LN overtime. *p* values from GEE. Bars indicate median values.

(E) Representative pictures of LN sections over time after 4$^{th}$ vaccination (scale bar: 500 μm) to illustrate the *in situ* quantification (right upper panel) performed on the germinal center (GC) and B cell follicle (BCF) percentage of area per tissue section at D3/4, D8, and D22 post-vaccination. The ratio GC/BCF was determined *in situ* at D3/4, D8, and D22. GCs were identified based on morphology as well as CD20, Ki67 expression, and T cell markers to localize dark zone and T cell zone (TCZ) (right lower panel). *p* values from GEE. Bars indicate mean values.

changes overtime in all animals upon vaccination (Figure 4C). The HLA-DR$^{pos}$Lin$^{neg}$ cell cluster, representing HLA-DR$^+$ myeloid cells, trended to expand in blood as early as D3/4, followed by a recovery by D8. In LN, the HLA-DR$^+$ myeloid cells expanded significantly with a peak by D8 and remained elevated, indicating a temporally distinct response in blood and LN; a similar trend was observed in LN for the CD123$^-$CADM1$^+$cDC1 and CD123$^-$ CD1c$^+$ cDC2[54,55] subsets, whereas in blood, the CD123$^-$CADM1$^+$ cDC1 levels increased at D8 and CD123$^-$ CD1c$^+$cDC2 levels decreased at D3/4 (Figure S4A). A transient change of B and

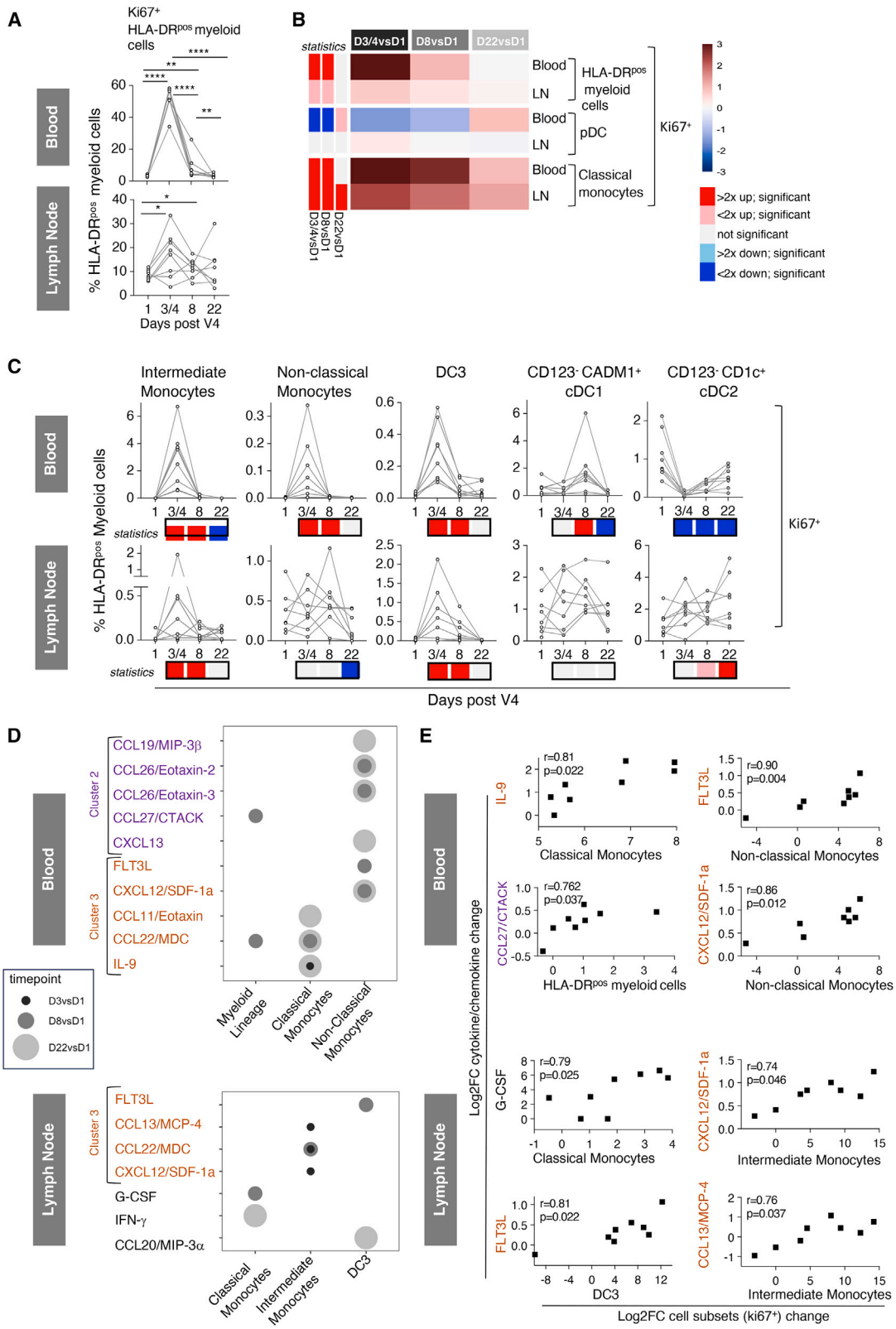


*(legend on next page)*

T cells was also observed. Both B and T cells transiently decreased in blood, with T cells recovering by D8 and B cells by D22. Conversely, after an initial decrease, an increase in T cells in the blood was paralleled by a significant decrease in LN. In LN, B cells trended toward a transient increase by D3/4 and recovered by D8, whereas T cells significantly decreased by D8 and recovered by D22. The dynamic change of lymphocyte frequencies resulted in an inverted B:T cell ratio comparing LN and blood (Figure 4D). These data are reminiscent of the LN activation found upon IL-7 treatment in macaques.[47] The change in T cells was meditated by both $CD4^+$ and $CD8^+$T cells (Figure S4B). Thus, DNA/LION vaccination resulted in a rapid and transient expansion and mobilization of PBMC and LNMC, affecting their trafficking within lymphoid and peripheral compartments.

Using high-plex *in situ* spatial phenotyping, we observed a significant increase in the size of the B cell follicle area and GC over time. These changes were visualized by immunohistochemistry using representative full LN tissue sections (Figure 4E, left panels) and supported by quantification (Figure 4E, right panels). We observed a significant increase of the B cell follicle areas (Figure 4E, right upper panel) and a significant increase in the number of activated GC, defined by $Ki67^+$-CD20 and B Cell Follicles (BCFs) morphology, presented as ratio of activated versus non-activated B cell follicles (Figure 4E, right lower panel). Together, *in situ* immunohistochemistry and flow cytometry analysis showed a significant increase in LN activation.

## Effect of DNA/LION vaccination on myeloid lineage cells in blood and lymph nodes

Different myeloid cell populations, in addition to $CD123^-CADM1^+$ cDC1 and $CD123^-$ $CD1c^+$cDC2, were monitored after vaccination, including classical, intermediate, and non-classical monocytes, plasmacytoid dendritic cells (pDCs) and the recently described dendritic cell type 3 (DC3[56]) (Figures 5A–5C and S5). We found significant changes by D3/4 analyzing different cell subsets. DNA/LION mediated an expansion of proliferating ($Ki67^+$) $HLA\text{-}DR^+$ myeloid cells in blood, and in 5 of 8 animals in LN (Figures 5A and 5B). Classical monocytes showed the largest expansion in blood and LN, in support of their essential role in the early inflammatory responses (Figures 5B and S5A). A significant increase in $CD14^+CD16^+$ monocyte subsets was found in blood and LN, and an increase in proliferating non-classical monocyte in blood (Figure 5C). pDC decreased in blood and returned to baseline only at D22 (Figures 5B and S5A). DC3, which play a crucial role in shaping $CD8^+$T cell responses,[57] significantly increased in both blood and LN (Figure 5C). Additionally, $Ki67^+CD123^-CADM1^+$cDC1 levels increased at D8 before returning to levels below baseline by D22, whereas $Ki67^+CD123^-$ $CD1c^+$cDC2 levels decreased at D3/4 and similarly rebounding but remaining below baseline by D22 (Figure 5C). Conversely, in LN, proliferating $CD123^-CADM1^+$cDC1 did not consistently change over time, while $CD123^-CD1c^+$cDC2 modestly increased with a slower kinetic at D8 and D22 (Figure 5C). The transient reduction of pDC and cDC in blood, accompanied by a simultaneous increase of DC3 in both compartments (Figures 5B and S5A), suggested a coordinated movement of DC to antigen-presented sites (Figures 5B and S5A). This movement predicted facilitation of initiating and boosting of adaptive immune responses within the lymphoid tissues. The changes of the proportions of the different cell subsets among proliferating $HLA\text{-}DR^+$ myeloid cells are summarized in Figure S5B.

Interestingly, we found several significant associations between the changes in myeloid cell subsets and changes (Log2FC; D2-D1) of plasma cytokines/chemokines. Significant associations, mainly from clusters 2 and 3, with changes in myeloid cell subsets are summarized in a bubble plot (Figure 5D) with selected correlations shown in Figure 5E. CCL13/MCP-4, CCL27/CTACK, CXCL12/SDF-1a, FLT3L, G-CSF, IL-9, and IFN-$\gamma$ correlated with increases in different proliferating myeloid subsets and DC. Several of these analytes play a role in myeloid and DC function and/or are produced by these cells.[49,58–64] These analytes are also associated with LN activation.[45–48,65] Several analytes were associated with cell expansion, function and or trafficking, i.e., G-CSF with classical monocytes,[66] FLT3L with DC3 and non-classical monocytes,[49,50] IL-9 with classical monocytes expansion,[67] CCL13/MCP-4 and monocytes, T cells and immature DC,[68] and CXCL12/SDF-1a with the $CD14^+CD16^+$ intermediate monocyte subset.[69] Association with antigen-presenting cells supports facilitation of adaptive immunity development resulting from a complex interplay among cytokines/chemokines and myeloid cells and lymphocytes.

## Increase of lymphocytes in lymph nodes correlates with innate immune responses

To gain a better understanding of the effect of DNA/LION vaccination on the GC, we examined different LN cell subsets. The distribution and dynamic changes of total proliferating ($Ki\text{-}67^+$) CD4 T follicular helper (Tfh; $CXCR5^+PD\text{-}1^{int}$), CD4 GC-Tfh ($CXCR5^+PD\text{-}1^{high}$), CD8 T follicular cells (Tfc1; $CXCR5^+PD\text{-}1^{int/high}$)[70–74] as well as GC-B cells ($Bcl\text{-}6^+CCR6^+$) are shown in

**Figure 5. DNA/LION vaccination promotes the proliferation and trafficking of myeloid cells**

(A) Proliferating $HLA\text{-}DR^+$ myeloid cell subsets in blood and LN after V4, expressed as percentage of total $HLA\text{-}DR^+$ myeloid cells. Bars indicate mean values. *p* values from GEE and are defined as $\leq$0.05, *; $\leq$0.01, **; $\leq$0.001, ***; $\leq$0.0001,****.

(B) Heatmap showing the Log2FC estimate from GEE of different proliferating cell subsets measured as percentage of $HLA\text{-}DR^+$ myeloid cells over time in blood and LN. Statistical analysis as in (A) is summarized in the left columns with significant increase (red) and decrease (blue) with >2x and <2x upregulation are shown in respective shades.

(C) Plots show proliferating myeloid cell subsets in blood and LN over time as percentage of $HLA\text{-}DR^+$ myeloid cells. Statistical analysis as in (A) and (B) is depicted below the graphs.

(D) Bubble plots show Spearman correlation ($p < 0.05$) between proliferating myeloid subsets (log2FC) and selected biomarkers (log2FC) in blood and LN, at D3/4 or D8 vs. D1. Time points indicated by different bubble size.

(E) Selected correlation plots from (D) in blood for classical monocytes (D3/4 vs. D1) and $HLA\text{-}DR^+$ myeloid cells and non-classical monocytes (D8 vs. D1) in LN for intermediate monocytes (D3/4 vs. D1) and for classical monocytes and DC3 (D8 vs. D1).

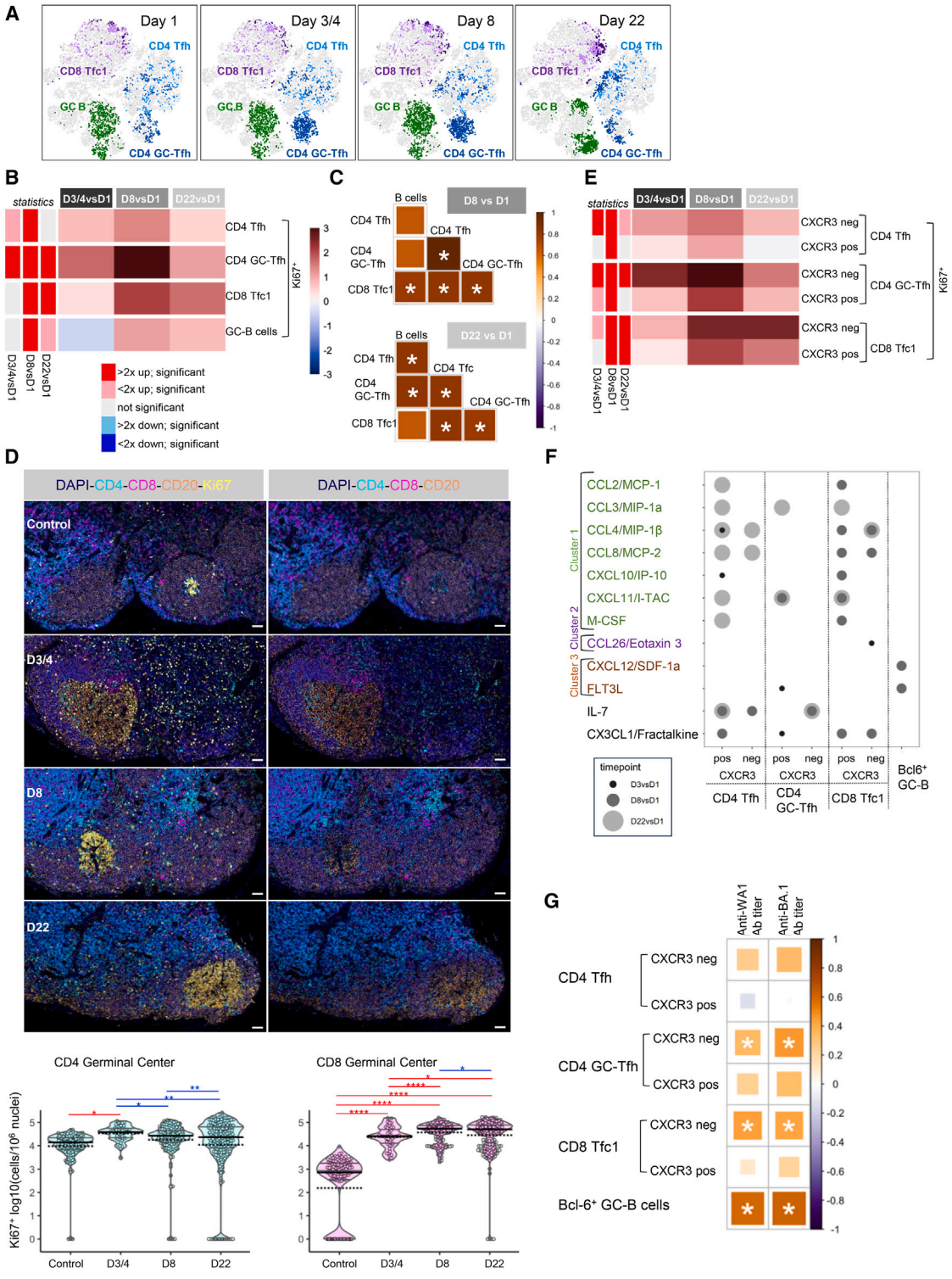


**Figure 6. DNA/LION vaccination induces germinal center activation**

(A) Proliferating LN cell subsets based on unsupervised t-SNE clustering of Ki67$^+$ live cells (gray background) with overlaid manually gated CD4 Tfh (CD3$^+$CD4$^+$CXCR5$^+$PD-1$^{int}$; light blue), CD4 GC-Tfh (CD4$^+$CD3$^+$CXCR5$^+$PD-1$^{high}$; dark blue), CD8 Tfc1 (CD3$^+$CD8$^+$CXCR5$^+$PD-1$^{int/high}$ [purple] with PD-1$^{high}$ fraction [darker purple]), and GC-B (CD3$^-$CD20$^+$CXCR5$^+$CCR6$^+$Bcl-6$^+$; green) cells.

(B) Heatmap showing Log2FC estimate from GEE of LN subsets. *p* values from GEE summarized in the left columns with significant increase (red) and decrease (blue) with >2x and <2x upregulation are shown in respective shades.

*(legend continued on next page)*

the t-SNE map as distinct clusters (Figure 6A) and by manual gating (Figures 6B and S6). All subsets significantly increased upon DNA/LION vaccination reaching peak levels by D8, with some subsets maintaining elevated proliferation through D22, although at lower level (Figure 6B). Interestingly, significant direct correlations were found among the changes of these lymphocyte subsets (Log2FC, D8 vs. D1; D22 vs. D1) (Figure 6C), supporting their coordinated increase.

High-plex immunofluorescence staining of LN visualized the changes of proliferating $CD4^+$ and $CD8^+$T cells over time after V4 (Figure 6D). Proliferating T cells were quantified (Figure 6D, lower panels) within activated (GC) and non-activated (non-GC) B cell follicles as well as in the T cell zone (TCZ) and compared to control animals naive to the LION vaccine (Figure S6B). Both $CD4^+$ and $CD8^+$ T cells increased in all areas of the LN at D3/4 compared to unvaccinated animals. The increase of $CD4^+$ T cells within GC was a rapid and transient response post vaccination shown by number of $CD4^+$T cells returning to baseline level by D8. Interestingly, the $CD8^+$T cells increased more drastically in BCF (GC and non-GC) than in TCZ, and showed a constant increase over time, maintaining a significantly higher number in all LN compartments than the unvaccinated animals. Thus, DNA/LION vaccination significantly expanded cell subsets known to play a pivotal role in the GC formation, providing help to the B cells and enhancing Ab production[75] upon changing their distribution within LN.

We conducted a more detailed analysis of GC T cells considering their expression of CXCR3, a chemokine receptor mainly effectors on T cells, known to play a role in trafficking,[76,77] but also in regulation of their interaction with antigen-presenting cells (APCs) mediating their differentiation.[78,79] $CXCR3^{neg}$ subsets significantly increased overtime, indicative of their potential retention in LN (Figures 6E and S6C). The $CXCR3^{pos}$ subsets expanded by D8, followed by a contraction of CD4 Tfh and CD4 GC-Tfh by D22, indicating their trafficking from the LN. On the other hand, the $CXCR3^{pos}$ CD8 Tfc1 cells remained at higher level at D22, indicating their distinct migration kinetics.

The CD4 Tfh, CD4 GC-Tfh and CD8 Tfc1 cell subsets (Figure S6D) exhibited a central memory phenotype ($CD28^+$ $CD95^+$). CCR7 was detected in a subset of CD4 Tfh cells, whereas CCR6 expression was primarily found in the GC-B cells. The lineage transcription factors Bcl-2 and Bcl-6 were differentially expressed in the four subsets, with expression of Bcl-2 predominantly in Tfh and Tfc cells, and Bcl-6 in GC-B cells and in a subset of CD4 GC-Tfh cells.

Next, we performed a correlation analysis between the chemokine/cytokine changes (D2 vs. D1, Log2FC) and changes of lymph nodes cell subsets overtime (Figures 6F and S7). Several of these analytes were also found to coordinately increase upon DNA/LION vaccination (see clusters in Figure 3C) and are known to serve as biomarkers for LN activation and induction of adaptive immune responses. Significant associations of $CXCR3^{pos}$ CD4 Tfh, CD4 GC-Tfh and CD8 Tfc1 cells were identified with cytokines/chemokines from cluster 1, belonging to the previously identified IL-15 signature,[51–53] associated with Ab development in mRNA/LNP vaccinated humans (see Figure 3C). $CXCR3^{pos}$ cell associations with CXCL10/IP-10, CXCL11/I-TAC (cluster 1) and CXCL12/SDF-1a (cluster 3) is supporting their migration from LN.[80] CXCL12/SDF-1a and FLT3L associations with Bcl-$6^+$ GC-B cells also support LN activation as these analytes play a role in B cell development, function and Ab production.[45–48,65] Associations of CD4 Tfh and CD4 GC-Tfh with IL-7 and associations of CD4 Tfh, CD4 GC-Tfh and CD8 Tfc1 with CX3CL1/Fractalkine reflected LN activation and trafficking.[47,63,64]

The observed changes in LN cell subsets and cytokine/chemokines indicate a connection between innate responses and adaptive T and B cell responses. Indeed, we also found direct associations between the levels of GC-B cells as well as of $CXCR3^{neg}$ CD4 GC-Tfh, an LN subset mainly involved in the GC formation, as well as CD8 Tfc1 cells and Ab levels measured over time (Figure 6G). Together, these data provided a critical link demonstrating the connection of DNA/LION-induced cytokine/chemokine changes, cell expansion and trafficking, strong LN activation and Ab development.

## Expansion of CD8 T cell memory subsets in draining LNs and blood

DNA/LION vaccination induced mainly antigen-specific $CD8^+$ T cell responses including memory responses (Figure 2), prompting the characterization of the vaccination effect on general proliferating ($Ki67^+$) $CD8^+$ naive and memory T cell population ($T_{EM}$, $T_{CM}$), as well as on CD8 Tfc1 in LN and circulating CD8 cTfc1 cells (Figures 7 and S8).

Pie charts illustrate the relative proportion of these 4 subsets within $CD8^+$ T cells (Figure 7A). As expected, the frequencies of naive, $T_{CM}$, and $CD8^+$ Tfc1 cells were higher in LN compared to blood at all time points. Conversely, the frequency of $T_{EM}$ was higher in blood reaching 66% of systemic $CD8^+$ T cells by D22, consistent with their role in immune surveillance and their effector functions.[81] In contrast, in LN, the frequency of $T_{EM}$ remained constant with ~14% (D1 to D22).

We identified a subset of CD8 Tfc3 cells ($CXCR5^+PD\text{-}1^{high}$) in LN, which showed similarity to CD4 GC-Tfh. We confirmed co-expression of Bcl-6 and ICOS in this fraction of CD8 Tfc3

(C) Direct correlations between the changes (Log2FC D8 and D22 vs. D1) of the listed populations. Color and size of square represent Spearman R, and asterisks indicate spearman $p < 0.05$.

(D) Representative pictures of activated CD4, CD8, and CD20 populations showing a B cell follicle (BCF), germinal center (GC), and T cell zone (TCZ) within an LN. Scale bars: 100 μm. *In situ* quantification of activated CD4 ($CD3^+CD4^+Ki67^+$) and CD8 ($CD3^+CD8a^+CD4^-Ki67^+$) T cells within GC in LN per million nuclei. Combined data points from 7 animals and 3 controls. Number of analyzed GC: control, 144; D3/4, 46; D8, 155; D22, 219. *p* values from linear mixed effect model. Mean and SEM are shown. The *p* values are defined as ≤0.05, *; ≤0.01, **; ≤0.001, ***; ≤0.0001,****.

(E) Heatmap showing Log2FC estimate from GEE of LN subsets +/− CXCR3. Statistical analysis as in (B).

(F) Bubble plot summarizing Spearman correlations ($p < 0.05$) between LN cell subset changes (log2FC, indicated by different bubble size) and the Log2FC of plasma cytokines/chemokines (D2 vs. D1).

(G) Correlation plots summarize spearman correlations of GC cell subset frequencies and Ab levels to WA1 (left) and BA.4/5 (right) over time. Color and size of square represent Spearman R, and asterisks indicate $p < 0.05$.

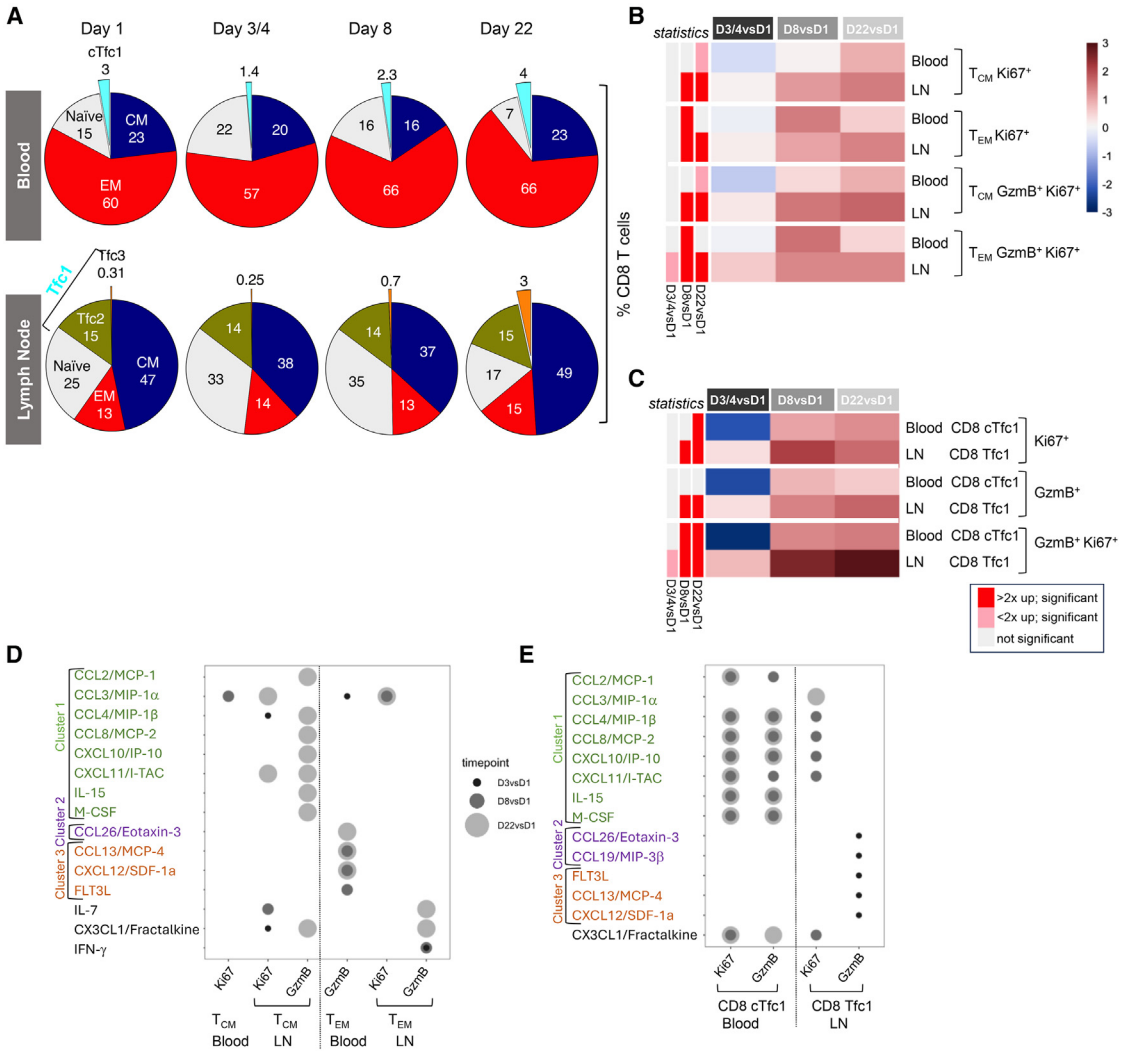


**Figure 7. DNA/LION vaccination affects CD8 cell subpopulations**

(A) Pie charts depict the mean frequency in blood and LN of manually gated $T_{EM}$ ($CD28^+CD95^+$), central memory ($T_{CM;}$ $CD28^-CD95^+$), and naive ($CD28^+CD95^-$) $CD8^+$T cell subsets and the circulating $CXCR5^+PD\text{-}1^{int/high}$ CD8 cTfc1 and the two LN-associated $CXCR5^+PD\text{-}1^{int}$ CD8 Tfc2 and $CXCR5^+$ $PD\text{-}1^{high}$ CD8 Tfc3 subsets.

(B) Heatmap shows manually gated Log2FC estimates from GEE of $Ki67^+$ and $Ki67^+GzmB^+$ $T_{CM}$ and $T_{EM}$ in blood and LN. *p* values from GEE are summarized in the left columns with significant increase (red) and decrease (blue) with >2x and <2x upregulation shown in respective shades.

(C) Heatmap shows manually gated Log2FC of CD8 cTfc1 in blood and CD8 Tfc1 in LN. Statistical analysis as in (B).

(D and E) Bubble plots summarizing Spearman correlation ($p = 0.05$)of changes in cell populations (Log2FC D3/4vsD1; D8vsD1, D22vsD1; indicated by different bubble sizes) and changes of plasma cytokines/chemokines (log2FC, D2 vs. D1) for (D) $T_{CM}$ and $T_{EM}$ and (E) CD8 cTfc1 in blood and CD8 Tfc1 in LN.

($CXCR5^+PD\text{-}1^{high}$) (Figure S8A), distinct from the circulating CD8 cTfc1 in blood. Also, like CD4 GC-Tfh, the CD8 Tfc1, Tfc2, and Tfc3 displayed a central memory phenotype, and the absence of CCR7 in blood and LN indicated a transitional memory ($T_{TM}$) phenotype associated with enhanced proprieties including the ability to proliferate and to exert effector functions in both lymphoid and systemic sites.[82] These data could emphasize the importance of CD8 Tfc3 ($CXCR5^+PD\text{-}1^{high}$) in exhibiting B cell helper function.[70,83]

The $CD8^+$T cell subsets were further tested for the proliferative capacity and/or cytotoxic potential. The proliferating ($Ki67^+$) $T_{CM}$ and $T_{EM}$ subsets increased transiently (D22 or D8, respectively) in the blood, but showed sustained increases in LN from D8 through D22 (Figure 7B). We also found that the $CD8^+$ Tfc1 subset[70–73,84] retained functional potential within the LN and circulation (Figure 7C), showing a significant increase of $Ki67^+GzmB^+$ cells by D8 and maintained through D22.

$T_{EM}$ and $T_{CM}$ (Figure S8B) were further characterized for expression of a series of different markers in both blood and LN. All CD8 subsets comprised a significant portion of cells expressing the lineage transcriptional factor Bcl-2, while lacking expression of Bcl-6, except for a small fraction of $CD8^+$ Tfc3,

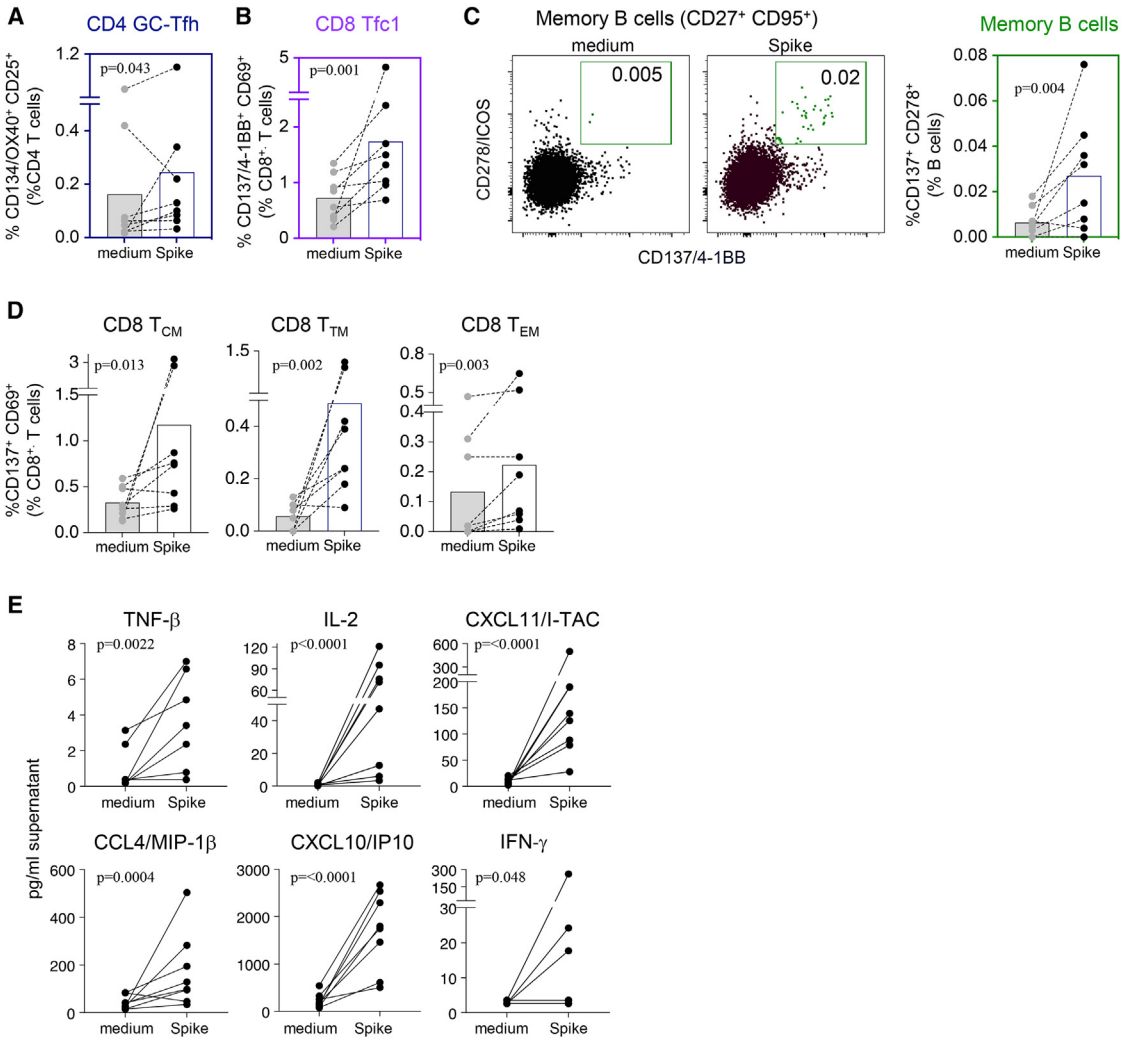


**Figure 8. Antigen-specific cell activation in LN by the AIM assay**

(A and B) Quantification of spike-specific (A) CD4 GC-Tfh and (B) CD8 Tfc1 cells by the AIM assay using LNMC isolated at D22 after 4th vaccination from DMSO- and spike peptide/protein-stimulated cells, respectively, showing activated (A) $CD25^+$ $CD134/OX40^+$ CD4 GC-Tfh and (B) $CD69^+$ $CD137/4\text{-}1BB^+$ CD8 Tfc1.

(C) Dot plot of a representative animal 43825 and data of all 8 animals, showing memory B cell activation (CD278/ICOS and CD137/4-1BB). Boxes indicate median values.

(D) Changes in spike-specific $CD8^+$ $T_{CM}$, $T_{TM}$, and $T_{EM}$ cells expressing CD137/4-1BB and the activation marker CD69.

(E) Cytokines/chemokines levels detected in the supernatant after 24 h incubation with medium or spike peptide/protein using the Meso Scale Discovery assay. *p* values were calculated by GEE.

associated with CD4 GC-Tfh and GC-B cells.[85,86] In blood, a large portion of $T_{EM}$ expressed T-bet compared to LN, supporting the important role of this transcription factor in the differentiation of CD8 and their acquisition of effector functions.

We found significant correlations between changes in several cytokines/chemokines (D2 vs. D1) and changes in CD8 memory (Figure 7D) and CD8 Tfc1 (Figure 7E) subsets. Changes of $CD8^+T_{CM}$ with cytotoxic potential (Figure 7D) were associated with IL-15, CCL2/MCP-1, CCL4/MIP-1β, CCL8/MCP-2, CXCL10/IP-10, CXCL11/I-TAC, M-CSF, analytes whose coordinated expression was reported in Figure 3C (cluster 1) and which are associated with T cell growth and migration.[87] Increase of $T_{EM}$ in blood correlated with CCL13/MCP-4, CXCL12/SDF-1a and FLT3L (cluster 3, Figure 3C), whereas both $T_{CM}$ and $T_{EM}$ in LN correlated with CX3CL1/Fractalkine (cluster 1) and IL-7, comprising analytes associated with LN activation.[45–48,65]

Changes of CD8 cTfc1 (Figure 7E) also showed a strong correlation with the IL-15 cluster (cluster 1) identified in Figure 3C. The CD8 Tfc1 in LN associated with the Eotaxin-3, CCL19/MIP-3b cluster (cluster 2) and with the FLT3L, CCL13/MCP-4, CXCL12/SDF-1a cluster (cluster 3) (see Figure 3C). Both subsets were associated with changes in CX3CL1/Fractalkine.

Together, these data showed that the vaccine-mediated cytokine/chemokine responses and their coordinated increases contributed to the significant changes in magnitude, phenotype and trafficking of different $CD8^+$ cell subsets in both blood and

LN. DNA/LION promoted the induction of T cell subsets with cytotoxic potential. Together, the induction of follicular helper CD4 subsets in LN (Figure 6) as well as follicular CD8 T cells (Figure 7) and GC-B cells (Figure 6) correlated with distinct cytokine/chemokine signatures providing a critical role for the development of humoral immune responses (Figure 6G).

### Detection of antigen-specific cellular responses in lymph nodes by AIM assay

In addition to the overall activation of lymphocyte subsets in LN upon DNA/LION vaccination (Figures 6 and 7), we further investigated their antigen-specific nature. Antigen-specific responses were measured *in vitro* in LNMC from draining LN by the activation-induced marker (AIM) assay[88] upon spike stimulation (Figure 8). We found significant increases of spike-activated CD4 GC-Tfh (CD134/OX40$^+$CD25$^+$; Figure 8A) and CD8 Tfc1 (CD137/4-1BB$^+$CD69$^+$; Figure 8B). We also found a significant increase in CD278/ICOS$^+$CD137/4-BB$^+$ double-positive memory (CD27$^+$CD95$^+$) B cells (Figure 8C). In addition, we found significant increases of spike-specific activated (CD137$^+$ICOS$^+$ [inducible T cell costimulator]) CD8$^+$ memory subsets ($T_{CM}$, $T_{TM}$, $T_{EM}$) (Figure 8D). Together, these data demonstrate the presence of antigen-specific activated T and B cell subsets in LN (Figure 8) and in blood (Figure 2).

Cytokines/chemokines secreted in the AIM assay were measured by multiplex immunoassay. We found significant production of TNF-β, IL-2, and CXCL11, and a trend and/or only few responders for CXCL10, CCL4/MIP-1β, and IFN-γ (Figure 8E), supporting spike-specific induction of Th1-associated chemokines. Together, DNA/LION vaccination resulted in induction of antigen-specific activated T cells both in blood (Figure 2) and in lymph node GC (Figure 8).

## DISCUSSION

In this study, we demonstrate that LION nanoparticle is a promising delivery technology for effective DNA vaccination by IM administration in macaques. Using SARS-CoV-2 spike DNA as a model, we found that DNA/LION vaccination induces cellular and humoral immune responses with durability maintained for >2 years after only 2 vaccinations, supporting a promising aspect of this vaccine regimen. The DNA/LION vaccine induced antibody responses significantly higher than naked DNA and comparable to DNA delivered by EP alone or co-immunized with adjuvanted protein,[32] a regimen known to maximize Ab levels in macaques.[16,34,35] Interestingly, we found that DNA/LION vaccination induced also very strong antigen-specific CD8$^+$T cell responses that exceeded the high level of CD4$^+$T cells. This feature is distinct from the more pronounced CD4$^+$T cell response obtained upon IM delivery of the same DNA direct or via EP including in clinical trials.[14,89,90] It is also different than that obtained by mRNA/LNP,[91] which induces moderate cellular responses with a preponderance of CD4$^+$ T cells.[92] In addition to blood, antigen-specific T cells were found also in LN by the AIM assay, supporting the potency of the DNA/LION vaccine resulting in antigen-specific cellular responses both in LN and blood. DNA/LION vaccination induces a unique and strong transient activation of cytokine/chemokines that can contribute to the development of robust vaccine-induced adaptive immune responses. Indeed, our data provided a critical link demonstrating the connection of DNA/LION-induced cytokine/chemokine changes, cell expansion and trafficking, strong LN activation and Ab development. Thus, the DNA/LION vaccine triggers all the critical events and is a promising platform to induce also humoral immune responses to more difficult immunogens, like HIV Env.

We also found that the DNA/LION vaccine induces rapid transient cytokine/chemokine responses within 4 h. Several of these were found to be coordinately regulated upon DNA/LION vaccination and are known to serve as a predictor for LN activation and induction of adaptive immune responses. Interestingly, the changes of several cytokine/chemokine showed an interrelation, grouped in 3 main clusters (Figure 3C), exemplified by IL-15 (cluster 1), CXCL13 (Cluster 2) and SDF1a-FLT3L (Cluster 3). We previously reported that several analytes present in cluster 1, including IL-15, CXCL10/IP-10, CCL3/MIP-1α, CCL4/MIP-1β, CCL22/MDC-1, were part of a signature associated with enhanced humoral immune responses in Pfizer/BioNTech BNT162b2 mRNA vaccinated persons.[51–53] This signature included IL-15, IFN-γ, IP-10/CXCL10, TNF-α and IL-6[51,52], and correlated with effective humoral immunity development whereas its absence in immunocompromized patients led to failure to develop Ab.[52,53] Thus, successful development of an anti-spike immune response in mRNA/LNP vaccinated humans was associated with activation of an IL-15 signature. Interestingly, DNA/LION vaccination in macaques induces a signature sharing similarities with that induced by mRNA/LNP in humans. Expanding this observation, our extensive immune phenotyping of DNA/LION vaccinated macaques (Figures 4, 5, 6, 7, and 8) allowed us to further analyze this finding. We found that expansion of different myeloid subsets and DC correlated with several cytokine/chemokines primarily from clusters 2 and 3, which play a role in myeloid and DC function and/or are produced by these cells.[49,58–64] Notably, an increase in G-CSF, providing important survival and activation signals to monocyte/macrophages,[66] was associated with an increase in the classical monocytes in LN. We also found significant associations between DC3 in LN and blood and non-classical monocytes with increase of FLT3L, a cytokine crucial for the development of both classical and plasmacytoid DC, supporting their growth and function.[49,50] IL-9, known for its role in monocyte expansion and recruitment,[67] correlated with an increase in classical monocytes in blood. Additionally, CCL13/MCP-4, which induces migration of monocytes, T cells and immature DC[68] and of CXCL12/SDF-1a, which activates downstream pathways mediating migration and survival of lymphocytes and monocytes[69] were associated with the proliferation of the CD14$^+$CD16$^+$ intermediate monocyte subset in LN. Significant associations of CXCR3$^{pos}$ LN CD4 cells with IL-7 are supported by our reported IL-7-mediated LN activation.[47] These, along with CXCR3$^{pos}$ CD8 cells also associated with CX3CL1/Fractalkine, a driver of LN trafficking[63,64] with contribution to mucosal immunity development,[93] with FLT3L, a cytokine known to be associated with LN activation, playing a role in B cell development, function and Ab production,[46,49,50] and with a group of analytes (cluster 1) including MIPs, MCPs, CXCL10/IP-10, CXCL11/I-TAC, M-CSF belonging to the IL-15

signature.[51,52,94] Gradients of CXCL10/IP-10, CXCL11/I-TAC, CXCL12/SDF-1a mediate LN cell migration via CXCR3.[80] The GC-B:CXCL12/SDF-1a association supports their trafficking and GC formation.[65] FLT3L associated CD4 GC-Tfh and GC-B cell changes. In addition, association of CD8 memory and CD8 Tfc1 subsets and changes in several cytokines/chemokines are also associated with cell growth and migration. Together, several of these analytes were also found to coordinately increase upon DNA/LION vaccination and served as biomarkers for LN activation and induction of adaptive immune responses. Our data show that DNA/LION vaccination drives a complex interplay of cytokines with myeloid and lymphocyte subsets facilitating the mobilization of antigen-presenting cells and development of adaptive immunity. Importantly, we found connections between innate responses and adaptive T and B cell responses, and in addition we also found associations between GC-B cells and CXCR3$^{neg}$ CD4 GC-Tfh and CD8 Tfc1 cells with Ab. Thus, our data show that DNA/LION vaccination strongly activated critical LN immune cell subsets resulting in robust humoral and cellular immune responses.

Interestingly, DNA/LION vaccination induces CD8$^+$T cells with cytotoxic (GzmB) potential, which may be important for the maintenance of protective immunity. Several features support the conclusion of continuous activation and maintenance of cytotoxic potential of the DNA/LION-induced antigen-specific CD8$^+$T cells. In addition to cytokine production (IFN-$\gamma$ and TNF-$\alpha$), they are cytotoxic competent (CD107a$^+$GzmB$^+$) and have proliferative capacity (Ki67$^+$). Spike-activated CD8 Tfc1 (CXCR5$^+$PD-1$^{int/high}$) also increased in the LN. Cells homing to lymphoid follicles have been reported to have multifunctional capabilities, providing help to B cells and possessing cytotoxic potential.[82] Induction of such cells by vaccination may be beneficial for addressing a virus defense, such as against HIV/simian immunodeficiency virus (SIV), which find sanctuary in LN.[95–98] Thus, the DNA/LION vaccine offers unique advantages in improving quality of the vaccine-induced T cell response. This is further supported by the induction of antigen-specific cytotoxic (GzmB$^+$CD107$^+$) $T_{EM}$ effectors expressing T-bet, a transcriptional factor supporting their expansion, differentiation and maturation.[39] Therefore, the DNA/LION vaccine overcomes a major hurdle in the vaccine field, namely the generation of strong and effective cellular immunity with CD8$^+$T cell preponderance, providing an advantage against certain infections. It has been argued that appropriate levels of functional CD8$^+$T cells may be essential for suppressing or eliminating chronic infections and for providing a block of spreading infection at the portal of entry.[99]

In contrast to mRNA/LNP vaccines, which circulate throughout the body and are hepatotropic,[100,101] LION was shown to have localized biodistribution detectable only in the injected muscle,[25] enabling efficient antigen expression in myocytes and local antigen-presenting cells. A robust activation of myeloid cells was found by D3/4 after vaccination, supported by the rapid (within 4 h) and transient activation of several cytokines/chemokines detected in plasma. The expansion of myeloid cells, monocyte and DC subsets in blood and LN was concomitant with their potential to present antigens. Classical monocytes have been reported to have the ability to differentiate into monocyte-derived macrophages and DC and play an integral part in controlling inflammation in tissues,[102] acquiring antigen-presentation properties during inflammatory responses.[103] Other monocyte subsets, including CD14$^+$CD16$^+$ intermediate and non-classical monocytes, although initially present in low abundance in LN, showed a significant increase. It has been suggested that under inflammatory conditions, intermediate monocytes possess high capacity to present antigens in comparison to classical and non-classical monocytes, and it has been shown that the intermediate subset induces high proliferation [reviewed in (51)]. Similarly, DC play a crucial role in the immune response. Conventional cDC1 possess a significant intrinsic ability to cross-present antigens via major histocompatibility complex class I, thereby activating CD8$^+$T cells and promoting T helper type 1 (Th1).[104] DC3 exhibit high expression CD1c, which functions to display lipids on the cell surface of antigen-presenting cells for direct recognition by T cells.[105] These results highlight the multi-faceted effects of DNA/LION vaccination.

In addition to myeloid cells, DNA/LION also induced activation and trafficking of the lymphocytes in blood and LN including both T and B cells, resulting in an increase of B cells in the LN and their migration from the blood. This effect is similar to our previously reported effect of IL-7 cytokine treatment,[47] which also increased B cells in LN leading to increase of GC within the LN. DNA/LION induced significant activation within the LN and GC increasing CD4 Tfh, CD4 GC-Tfh, CD8 Tfc1 cells and Bcl-6$^+$ GC-B cells, as well as enlarged B cell follicles. We also found induction of a small subset of CD8 Tfc3, defined by CXCR5$^+$ PD-1$^{high}$, sharing key features with the CD4 GC-Tfh.[75] Importantly, their cytotoxic potential (GzmB$^+$) and proliferative capacity (Ki67$^+$) was significantly increased upon DNA/LION vaccination supporting their increased effector function.

It has been reported that immunity against SARS-CoV-2 generated after infection or after vaccination by the mRNA/LNP vaccines[52,106–110] wanes, requiring frequent boosts. In contrast, the spike DNA/LION vaccine generated noteworthy long-lasting sustained responses in macaques. It is therefore important to further expand these results and to study B cell maintenance and the generation and properties of plasma cells. Therefore, the present work is important in suggesting a vaccine formulation with important additional properties. Future studies probing the long-lasting localization and properties of immune cells, including mucosal sites and bone marrow will be important in evaluating the full potential of the presented methodology. LION does not require cold-chain and can be delivered by simple IM injection.[25–31] Vaccine preparation with just two components is scalable and predictable, avoiding complications of different protein and vector production, which may require manufacturing adjustments and regulatory hurdles.

In conclusion, DNA/LION is a promising platform for effective nucleic acid delivery for vaccination. DNA/LION formulation induced distinct cytokine/chemokine signatures that contributed to proliferation and trafficking of immune cell subsets and supported high magnitude of functional antigen-specific responses in LN and blood. This delivery method with its ability to induce robust T cell responses with cytotoxic potential, in addition to high neutralizing Ab has also the potential to be used in other vaccine efforts, including cancer immunotherapy.

## Limitations of the study

We show that DNA/LION vaccine induces robust and long-lasting humoral and cellular immune responses in macaques, using SARS-CoV-2 spike DNA as model immunogen. This established the proof-of-principle of this simple DNA delivery method. It remains to be explored whether the strong vaccine-induced immunity can be expanded to other immunogens and, thus be of general application. A limitation is the lack of a challenge after LION/DNA vaccination. However, the induced immune response is comparable to that of spike DNA delivered by EP either alone or co-immunized with protein, and is therefore predicted to be protective, as we showed in a previous challenge study.[32] Due to the approved mRNA/LNP vaccines (Moderna, Pfizer/BioNtech) for human use, and the known correlates of protection, we did not consider that a challenge with pathogenic SARS-CoV-2 would be justifiable at this point of time. Other DNA/LION vaccines need to be tested such as in the SIV/HIV model.

## RESOURCE AVAILABILITY

### Lead contact

Requests for further information and resources should be directed to and will be fulfilled by the lead contact, Barbara K. Felber (Barbara.felber@nih.gov).

### Materials availability

This study did not generate new unique reagents.

### Data and code availability

- Data needed to evaluate the conclusions in the paper are present in the paper and the supplementary materials and at GitHub: https://github.com/NCI-VB/felber_LION_macaque.
- Code has been deposited at GitHub: https://github.com/NCI-VB/felber_LION_macaque.
- Any additional information required to reanalyze the data reported in this article is available from the lead contact upon request.

## ACKNOWLEDGMENTS

We thank Y. Wang and J. Inglefield, Clinical Services Program, Frederick National Laboratory for Cancer Research, for Meso Scale Discovery assay performance; D. Esposito (Protein Expression Lab, Frederick National Laboratory for Cancer Research, NCI) for SARS-CoV-2 protein; D. Weiss, J. Treece, J. Misamore, H. Thomasson, M. Ferrari, and staff (BIOQUAL, Inc.) for excellent support with the macaque studies; J.E. for discussions; K.M. McKinnon for flow cytometry advice; A. Kane for graphic work support; and T. Jones for editorial assistance. The graphical abstract and Figure 1A were created with BioRender.com (MM, 2025, https://BioRender.com/d46d805).

This work was supported by funding from the Intramural Research Program, National Institutes of Health, National Cancer Institute, Center for Cancer Research, to B.K.F. This project has been funded in whole or in part with federal funds from the National Cancer Institute, National Institutes of Health, under contract no. 75N91019D00024/HHSN261201500003I. The content of this publication does not necessarily reflect the views or policies of the Department of Health and Human Services, nor does mention of trade names, commercial products, or organizations imply endorsement by the U.S. Government. The funders had no role in the experimental design, collection of data, or writing the paper.

## AUTHOR CONTRIBUTIONS

The study was conceptualized by B.K.F. and G.N.P. Supervision of the study was done by B.K.F., M.R., and G.N.P. Investigation was conducted by M.R., S.K., M.M., S.D., S.S., K.C.G., R.B., J.B., E.A.U., C.D., D.S., P.B., J.E., and A.P.K. Materials/formulation were done by A.P.K., P.B., and S.G.R. Formal analysis was performed by K.C.G., M.R., S.K., M.M., M.R., G.N.P., and B.K.F. Funding acquisition was done by B.K.F., S.G.R., and G.N.P. The following authors prepared the original draft with inputs from all coauthors: B.K.F., G.N.P., M.R., S.K., and M.M. All authors have read and agreed to the published version of the manuscript.

## DECLARATION OF INTERESTS

S.G.R., J.E., P.B., and A.P.K. are employees of HDT Bio Corp and as such receive compensation.

## STAR★METHODS

Detailed methods are provided in the online version of this paper and include the following:

- KEY RESOURCES TABLE
- EXPERIMENTAL MODEL AND STUDY PARTICIPANT DETAILS
  - Non human primates
- METHOD DETAILS
  - Vaccination
  - Cytokine/chemokine analysis
  - SARS-CoV-2 antibody measurements
  - Isolation of PBMC and preparation of single-cell suspensions from LNs
  - Antigen-specific T cell responses in blood
  - Immune cell phenotyping and flow cytometry
  - AIM assay
  - High-plex *in situ* spatial phenotyping analysis
- QUANTIFICATION AND STATISTICAL ANALYSIS

## SUPPLEMENTAL INFORMATION

Supplemental information can be found online at https://doi.org/10.1016/j.isci.2025.112232.

Received: August 30, 2024
Revised: February 15, 2025
Accepted: March 13, 2025
Published: March 18, 2025

## REFERENCES

1. Felber, B.K., Valentin, A., Rosati, M., Bergamaschi, C., and Pavlakis, G.N. (2014). HIV DNA Vaccine: Stepwise improvements make a difference. Vaccines *2*, 354–379.
2. Pardi, N., and Weissman, D. (2017). Nucleoside Modified mRNA Vaccines for Infectious Diseases. Methods Mol. Biol. *1499*, 109–121. https://doi.org/10.1007/978-1-4939-6481-9_6.
3. Armbruster, N., Jasny, E., and Petsch, B. (2019). Advances in RNA Vaccines for Preventive Indications: A Case Study of A Vaccine Against Rabies. Vaccines *7*, 132. https://doi.org/10.3390/vaccines7040132.
4. Sahin, U., Karikó, K., and Türeci, Ö. (2014). mRNA-based therapeutics–developing a new class of drugs. Nat. Rev. Drug Discov. *13*, 759–780. https://doi.org/10.1038/nrd4278.
5. Gebre, M.S., Brito, L.A., Tostanoski, L.H., Edwards, D.K., Carfi, A., and Barouch, D.H. (2021). Novel approaches for vaccine development. Cell *184*, 1589–1603. https://doi.org/10.1016/j.cell.2021.02.030.
6. Gary, E.N., and Weiner, D.B. (2020). DNA vaccines: prime time is now. Curr. Opin. Immunol. *65*, 21–27. https://doi.org/10.1016/j.coi.2020.01.006.
7. Liu, M.A. (2019). A Comparison of Plasmid DNA and mRNA as Vaccine Technologies. Vaccines *7*, 37. https://doi.org/10.3390/vaccines7020037.

8. Schalk, J.A.C., Mooi, F.R., Berbers, G.A.M., van Aerts, L.A.G.J.M., Ovelgönne, H., and Kimman, T.G. (2006). Preclinical and clinical safety studies on DNA vaccines. Hum. Vaccin. *2*, 45–53. https://doi.org/10.4161/hv.2.2.2620.

9. Broderick, K.E., and Humeau, L.M. (2017). Enhanced Delivery of DNA or RNA Vaccines by Electroporation. Methods Mol. Biol. *1499*, 193–200. https://doi.org/10.1007/978-1-4939-6481-9_12.

10. Flingai, S., Czerwonko, M., Goodman, J., Kudchodkar, S.B., Muthumani, K., and Weiner, D.B. (2013). Synthetic DNA Vaccines: Improved Vaccine Potency by Electroporation and Co-Delivered Genetic Adjuvants. Front. Immunol. *4*, 354. https://doi.org/10.3389/fimmu.2013.00354.

11. Morrow, M.P., and Weiner, D.B. (2008). Cytokines as adjuvants for improving anti-HIV responses. AIDS *22*, 333–338.

12. Jalah, R., Patel, V., Kulkarni, V., Rosati, M., Alicea, C., Ganneru, B., von Gegerfelt, A., Huang, W., Guan, Y., Broderick, K.E., et al. (2012). IL-12 DNA as molecular vaccine adjuvant increases the cytotoxic T cell responses and breadth of humoral immune responses in SIV DNA vaccinated macaques. Hum. Vaccin. Immunother. *8*, 1620–1629.

13. Edupuganti, S., De Rosa, S., Elizaga, M., Lu, Y., Han, X., Huang, Y., Swann, E., Polakowski, L., S, A.K., Keefer, M., et al. (2020). Intramuscular and Intradermal Electroporation of HIV-1 PENNVAX-GP((R)) DNA Vaccine and IL-12 Is Safe, Tolerable, Acceptable in Healthy Adults. Vaccines *8*, 741. https://doi.org/10.3390/vaccines8040741.

14. Elizaga, M.L., Li, S.S., Kochar, N.K., Wilson, G.J., Allen, M.A., Tieu, H.V.N., Frank, I., Sobieszczyk, M.E., Cohen, K.W., Sanchez, B., et al. (2018). Safety and tolerability of HIV-1 multiantigen pDNA vaccine given with IL-12 plasmid DNA via electroporation, boosted with a recombinant vesicular stomatitis virus HIV Gag vaccine in healthy volunteers in a randomized, controlled clinical trial. PLoS One *13*, e0202753. https://doi.org/10.1371/journal.pone.0202753.

15. Hu, X., Valentin, A., Cai, Y., Dayton, F., Rosati, M., Ramírez-Salazar, E.G., Kulkarni, V., Broderick, K.E., Sardesai, N.Y., Wyatt, L.S., et al. (2018). Rapid and High Recall of T Cell Responses upon DNA or rMVA Boost in Macaques Vaccinated with HIV/SIV Conserved Element CE gag DNA Vaccine. Hum. Gene Ther. *29*, 1029–1043.

16. Jalah, R., Kulkarni, V., Patel, V., Rosati, M., Alicea, C., Bear, J., Yu, L., Guan, Y., Shen, X., Tomaras, G.D., et al. (2014). DNA and protein co-immunization improves the magnitude and longevity of humoral immune responses in macaques. PLoS One *9*, e91550. https://doi.org/10.1371/journal.pone.0091550.

17. Patel, V., Valentin, A., Kulkarni, V., Rosati, M., Bergamaschi, C., Jalah, R., Alicea, C., Minang, J.T., Trivett, M.T., Ohlen, C., et al. (2010). Long-lasting humoral and cellular immune responses and mucosal dissemination after intramuscular DNA immunization. Vaccine *28*, 4827–4836. https://doi.org/10.1016/j.vaccine.2010.04.064.

18. Kulkarni, V., Rosati, M., Jalah, R., Ganneru, B., Alicea, C., Yu, L., Guan, Y., LaBranche, C., Montefiori, D.C., King, A.D., et al. (2014). DNA Vaccination by Intradermal Electroporation Induces Long-lasting Immune Responses in Rhesus Macaques. J. Med. Primatol. *43*, 329–340.

19. Kulkarni, V., Rosati, M., Bear, J., Pilkington, G.R., Jalah, R., Bergamaschi, C., Singh, A.K., Alicea, C., Chowdhury, B., Zhang, G.-M., et al. (2013). Comparison of Intradermal and Intramuscular Delivery of SIV Env DNA by in vivo Electroporation in Macaques. Hum. Vaccin. Immunother. *9*, 2081–2094.

20. Kulkarni, V., Rosati, M., Valentin, A., Jalah, R., Alicea, C., Yu, L., Guan, Y., Shen, X., Tomaras, G.D., LaBranche, C., et al. (2013). Vaccination with Vaxfectin® adjuvanted SIV DNA Induces Long-lasting Humoral Immune Responses Able to Reduce SIVmac251 Viremia. Hum. Vaccin. Immunother. *9*, 2069–2080.

21. Baden, L.R., El Sahly, H.M., Essink, B., Follmann, D., Neuzil, K.M., August, A., Clouting, H., Fortier, G., Deng, W., Han, S., et al. (2021). Phase 3 Trial of mRNA-1273 during the Delta-Variant Surge. N. Engl. J. Med. *385*, 2485–2487. https://doi.org/10.1056/NEJMc2115597.

22. Corbett, K.S., Flynn, B., Foulds, K.E., Francica, J.R., Boyoglu-Barnum, S., Werner, A.P., Flach, B., O'Connell, S., Bock, K.W., Minai, M., et al. (2020). Evaluation of the mRNA-1273 Vaccine against SARS-CoV-2 in Nonhuman Primates. N. Engl. J. Med. *383*, 1544–1555. https://doi.org/10.1056/NEJMoa2024671.

23. Walsh, E.E., Frenck, R., Falsey, A.R., Kitchin, N., Absalon, J., Gurtman, A., Lockhart, S., Neuzil, K., Mulligan, M.J., Bailey, R., et al. (2020). RNA-Based COVID-19 Vaccine BNT162b2 Selected for a Pivotal Efficacy Study. Preprint at medRxiv. https://doi.org/10.1101/2020.08.17.20176651.

24. Polack, F.P., Thomas, S.J., Kitchin, N., Absalon, J., Gurtman, A., Lockhart, S., Perez, J.L., Pérez Marc, G., Moreira, E.D., Zerbini, C., et al. (2020). Safety and Efficacy of the BNT162b2 mRNA Covid-19 Vaccine. N. Engl. J. Med. *383*, 2603–2615. https://doi.org/10.1056/NEJMoa2034577.

25. Kimura, T., Leal, J.M., Simpson, A., Warner, N.L., Berube, B.J., Archer, J.F., Park, S., Kurtz, R., Hinkley, T., Nicholes, K., et al. (2023). A localizing nanocarrier formulation enables multi-target immune responses to multivalent replicating RNA with limited systemic inflammation. Mol. Ther. *31*, 2360–2375. https://doi.org/10.1016/j.ymthe.2023.06.017.

26. Khandhar, A.P., Landon, C.D., Archer, J., Krieger, K., Warner, N.L., Randall, S., Berube, B.J., Erasmus, J.H., Sather, D.N., and Staats, H.F. (2023). Evaluation of repRNA vaccine for induction and in utero transfer of maternal antibodies in a pregnant rabbit model. Mol. Ther. *31*, 1046–1058. https://doi.org/10.1016/j.ymthe.2023.02.022.

27. Erasmus, J.H., Archer, J., Fuerte-Stone, J., Khandhar, A.P., Voigt, E., Granger, B., Bombardi, R.G., Govero, J., Tan, Q., Durnell, L.A., et al. (2020). Intramuscular Delivery of Replicon RNA Encoding ZIKV-117 Human Monoclonal Antibody Protects against Zika Virus Infection. Mol. Ther. Methods Clin. Dev. *18*, 402–414. https://doi.org/10.1016/j.omtm.2020.06.011.

28. Erasmus, J.H., Khandhar, A.P., Guderian, J., Granger, B., Archer, J., Archer, M., Gage, E., Fuerte-Stone, J., Larson, E., Lin, S., et al. (2018). A Nanostructured Lipid Carrier for Delivery of a Replicating Viral RNA Provides Single, Low-Dose Protection against Zika. Mol. Ther. *26*, 2507–2522. https://doi.org/10.1016/j.ymthe.2018.07.010.

29. O'Connor, M.A., Hawman, D.W., Meade-White, K., Leventhal, S., Song, W., Randall, S., Archer, J., Lewis, T.B., Brown, B., Fredericks, M.N., et al. (2023). A replicon RNA vaccine can induce durable protective immunity from SARS-CoV-2 in nonhuman primates after neutralizing antibodies have waned. PLoS Pathog. *19*, e1011298. https://doi.org/10.1371/journal.ppat.1011298.

30. O'Connor, M.A., Erasmus, J.H., Randall, S., Archer, J., Lewis, T.B., Brown, B., Fredericks, M., Groenier, S., Iwayama, N., Ahrens, C., et al. (2021). A Single Dose SARS-CoV-2 Replicon RNA Vaccine Induces Cellular and Humoral Immune Responses in Simian Immunodeficiency Virus Infected and Uninfected Pigtail Macaques. Front. Immunol. *12*, 800723. https://doi.org/10.3389/fimmu.2021.800723.

31. Saraf, A., Gurjar, R., Kaviraj, S., Kulkarni, A., Kumar, D., Kulkarni, R., Virkar, R., Krishnan, J., Yadav, A., Baranwal, E., et al. (2024). An Omicron-specific, self-amplifying mRNA booster vaccine for COVID-19: a phase 2/3 randomized trial. Nat. Med. *30*, 1363–1372. https://doi.org/10.1038/s41591-024-02955-2.

32. Rosati, M., Agarwal, M., Hu, X., Devasundaram, S., Stellas, D., Chowdhury, B., Bear, J., Burns, R., Donohue, D., Pessaint, L., et al. (2021). Control of SARS-CoV-2 infection after Spike DNA or Spike DNA+Protein co-immunization in rhesus macaques. PLoS Pathog. *17*, e1009701. https://doi.org/10.1371/journal.ppat.1009701.

33. Erasmus, J.H., Khandhar, A.P., O'Connor, M.A., Walls, A.C., Hemann, E.A., Murapa, P., Archer, J., Leventhal, S., Fuller, J.T., Lewis, T.B., et al. (2020). An Alphavirus-derived replicon RNA vaccine induces SARS-CoV-2 neutralizing antibody and T cell responses in mice and nonhuman primates. Sci. Transl. Med. *12*, eabc9396. https://doi.org/10.1126/scitranslmed.abc9396.

34. Felber, B.K., Lu, Z., Hu, X., Valentin, A., Rosati, M., Remmel, C.A.L., Weiner, J.A., Carpenter, M.C., Faircloth, K., Stanfield-Oakley, S., et al. (2020). Co-immunization of DNA and Protein in the Same Anatomical Sites Induces Superior Protective Immune Responses against SHIV Challenge. Cell Rep. *31*, 107624. https://doi.org/10.1016/j.celrep.2020.107624.

35. Li, J., Valentin, A., Kulkarni, V., Rosati, M., Beach, R.K., Alicea, C., Hannaman, D., Reed, S.G., Felber, B.K., Pavlakis, G.N., and Pavlakis, G.N. (2013). HIV/SIV DNA Vaccine Combined with Protein in a Co-immunization Protocol Elicits Highest Humoral Responses to Envelope in Mice and Macaques. Vaccine *31*, 3747–3755.

36. Rosati, M., Bergamaschi, C., Valentin, A., Kulkarni, V., Jalah, R., Alicea, C., Patel, V., von Gegerfelt, A.S., Montefiori, D.C., Venzon, D.J., et al. (2009). DNA vaccination in rhesus macaques induces potent immune responses and decreases acute and chronic viremia after SIVmac251 challenge. Proc. Natl. Acad. Sci. USA *106*, 15831–15836.

37. McLane, L.M., Ngiow, S.F., Chen, Z., Attanasio, J., Manne, S., Ruthel, G., Wu, J.E., Staupe, R.P., Xu, W., Amaravadi, R.K., et al. (2021). Role of nuclear localization in the regulation and function of T-bet and Eomes in exhausted CD8 T cells. Cell Rep. *35*, 109120. https://doi.org/10.1016/j.celrep.2021.109120.

38. Intlekofer, A.M., Takemoto, N., Wherry, E.J., Longworth, S.A., Northrup, J.T., Palanivel, V.R., Mullen, A.C., Gasink, C.R., Kaech, S.M., Miller, J.D., et al. (2005). Effector and memory CD8+ T cell fate coupled by T-bet and eomesodermin. Nat. Immunol. *6*, 1236–1244. https://doi.org/10.1038/ni1268.

39. Lazarevic, V., Glimcher, L.H., and Lord, G.M. (2013). T-bet: a bridge between innate and adaptive immunity. Nat. Rev. Immunol. *13*, 777–789. https://doi.org/10.1038/nri3536.

40. Mantovani, A., Savino, B., Locati, M., Zammataro, L., Allavena, P., and Bonecchi, R. (2010). The chemokine system in cancer biology and therapy. Cytokine Growth Factor Rev. *21*, 27–39. https://doi.org/10.1016/j.cytogfr.2009.11.007.

41. Mantovani, A., Sica, A., Sozzani, S., Allavena, P., Vecchi, A., and Locati, M. (2004). The chemokine system in diverse forms of macrophage activation and polarization. Trends Immunol. *25*, 677–686. https://doi.org/10.1016/j.it.2004.09.015.

42. Dillemans, L., De Somer, L., Neerinckx, B., and Proost, P. (2023). A review of the pleiotropic actions of the IFN-inducible CXC chemokine receptor 3 ligands in the synovial microenvironment. Cell. Mol. Life Sci. *80*, 78. https://doi.org/10.1007/s00018-023-04715-w.

43. Tahtinen, S., Tong, A.J., Himmels, P., Oh, J., Paler-Martinez, A., Kim, L., Wichner, S., Oei, Y., McCarron, M.J., Freund, E.C., et al. (2022). IL-1 and IL-1ra are key regulators of the inflammatory response to RNA vaccines. Nat. Immunol. *23*, 532–542. https://doi.org/10.1038/s41590-022-01160-y.

44. Cavalli, G., Colafrancesco, S., Emmi, G., Imazio, M., Lopalco, G., Maggio, M.C., Sota, J., and Dinarello, C.A. (2021). Interleukin 1alpha: a comprehensive review on the role of IL-1alpha in the pathogenesis and treatment of autoimmune and inflammatory diseases. Autoimmun. Rev. *20*, 102763. https://doi.org/10.1016/j.autrev.2021.102763.

45. Havenar-Daughton, C., Lindqvist, M., Heit, A., Wu, J.E., Reiss, S.M., Kendric, K., Bélanger, S., Kasturi, S.P., Landais, E., Akondy, R.S., et al. (2016). CXCL13 is a plasma biomarker of germinal center activity. Proc. Natl. Acad. Sci. USA *113*, 2702–2707. https://doi.org/10.1073/pnas.1520112113.

46. Petkau, G., and Turner, M. (2019). Signalling circuits that direct early B-cell development. Biochem. J. *476*, 769–778. https://doi.org/10.1042/BCJ20180565.

47. Pandit, H., Valentin, A., Angel, M., Deleage, C., Bergamaschi, C., Bear, J., Sowder, R., Felber, B.K., and Pavlakis, G.N. (2023). Step-dose IL-7 treatment promotes systemic expansion of T cells and alters immune cell landscape in blood and lymph nodes. iScience *26*, 105929. https://doi.org/10.1016/j.isci.2023.105929.

48. Choi, Y.S., Eto, D., Yang, J.A., Lao, C., and Crotty, S. (2013). Cutting edge: STAT1 is required for IL-6-mediated Bcl6 induction for early follicular helper cell differentiation. J. Immunol. *190*, 3049–3053. https://doi.org/10.4049/jimmunol.1203032.

49. Cueto, F.J., and Sancho, D. (2021). The Flt3L/Flt3 Axis in Dendritic Cell Biology and Cancer Immunotherapy. Cancers *13*, 1525. https://doi.org/10.3390/cancers13071525.

50. Wilson, K.R., Villadangos, J.A., and Mintern, J.D. (2021). Dendritic cell Flt3 - regulation, roles and repercussions for immunotherapy. Immunol. Cell Biol. *99*, 962–971. https://doi.org/10.1111/imcb.12484.

51. Bergamaschi, C., Terpos, E., Rosati, M., Angel, M., Bear, J., Stellas, D., Karaliota, S., Apostolakou, F., Bagratuni, T., Patseas, D., et al. (2021). Systemic IL-15, IFN-gamma, and IP-10/CXCL10 signature associated with effective immune response to SARS-CoV-2 in BNT162b2 mRNA vaccine recipients. Cell Rep. *36*, 109504. https://doi.org/10.1016/j.celrep.2021.109504.

52. Rosati, M., Terpos, E., Homan, P., Bergamaschi, C., Karaliota, S., Ntanasis-Stathopoulos, I., Devasundaram, S., Bear, J., Burns, R., Bagratuni, T., et al. (2023). Rapid Transient and Longer-Lasting Innate Cytokine Changes Associated with Adaptive Immunity after Repeated SARS-CoV-2 BNT162b2 mRNA Vaccinations. Front. Immunol. *14*, 1292568. https://doi.org/10.3389/fimmu.2023.1292568.

53. Bergamaschi, C., Pagoni, M., Rosati, M., Angel, M., Tzannou, I., Vlachou, M., Darmani, I., Ullah, A., Bear, J., Devasundaram, S., et al. (2022). Reduced Antibodies and Innate Cytokine Changes in SARS-CoV-2 BNT162b2 mRNA Vaccinated Transplant Patients With Hematological Malignancies. Front. Immunol. *13*, 899972. https://doi.org/10.3389/fimmu.2022.899972.

54. Gardet, M., Haigh, O., Meurisse, F., Coindre, S., Dimant, N., Desjardins, D., Bourgeois, C., Goujard, C., Vaslin, B., Relouzat, F., et al. (2024). Identification of macaque dendritic cell precursors in blood and tissue reveals their dysregulation in early SIV infection. Cell Rep. *43*, 113994. https://doi.org/10.1016/j.celrep.2024.113994.

55. Sugimoto, C., Hasegawa, A., Saito, Y., Fukuyo, Y., Chiu, K.B., Cai, Y., Breed, M.W., Mori, K., Roy, C.J., Lackner, A.A., et al. (2015). Differentiation Kinetics of Blood Monocytes and Dendritic Cells in Macaques: Insights to Understanding Human Myeloid Cell Development. J. Immunol. *195*, 1774–1781. https://doi.org/10.4049/jimmunol.1500522.

56. Villani, A.C., Satija, R., Reynolds, G., Sarkizova, S., Shekhar, K., Fletcher, J., Griesbeck, M., Butler, A., Zheng, S., Lazo, S., et al. (2017). Single-cell RNA-seq reveals new types of human blood dendritic cells, monocytes, and progenitors. Science *356*, eaah4573. https://doi.org/10.1126/science.aah4573.

57. Bourdely, P., Anselmi, G., Vaivode, K., Ramos, R.N., Missolo-Koussou, Y., Hidalgo, S., Tosselo, J., Nuñez, N., Richer, W., Vincent-Salomon, A., et al. (2020). Transcriptional and Functional Analysis of CD1c(+) Human Dendritic Cells Identifies a CD163(+) Subset Priming CD8(+) CD103(+) T Cells. Immunity *53*, 335–352.e8. https://doi.org/10.1016/j.immuni.2020.06.002.

58. Momenilandi, M., Levy, R., Sobrino, S., Li, J., Lagresle-Peyrou, C., Esmaeilzadeh, H., Fayand, A., Le Floc'h, C., Guerin, A., Mina, E.D., et al. (2024). FLT3L governs the development of partially overlapping hematopoietic lineages in humans and mice. Cell *187*, 2817–2837.e31. https://doi.org/10.1016/j.cell.2024.04.009.

59. Kim, S.W., Choi, S.M., Choo, Y.S., Kim, I.K., Song, B.W., and Kim, H.S. (2015). Flt3 ligand induces monocyte proliferation and enhances the function of monocyte-derived dendritic cells in vitro. J. Cell. Physiol. *230*, 1740–1749. https://doi.org/10.1002/jcp.24824.

60. Anandasabapathy, N., Breton, G., Hurley, A., Caskey, M., Trumpfheller, C., Sarma, P., Pring, J., Pack, M., Buckley, N., Matei, I., et al. (2015). Efficacy and safety of CDX-301, recombinant human Flt3L, at expanding dendritic cells and hematopoietic stem cells in healthy human volunteers. Bone Marrow Transplant. *50*, 924–930. https://doi.org/10.1038/bmt.2015.74.

61. Garcia-Zepeda, E.A., Combadiere, C., Rothenberg, M.E., Sarafi, M.N., Lavigne, F., Hamid, Q., Murphy, P.M., and Luster, A.D. (1996). Human monocyte chemoattractant protein (MCP)-4 is a novel CC chemokine with activities on monocytes, eosinophils, and basophils induced in allergic and nonallergic inflammation that signals through the CC chemokine receptors (CCR)-2 and -3. J. Immunol. *157*, 5613–5626.

62. Bogdan, C., and Schleicher, U. (2006). Production of interferon-gamma by myeloid cells–fact or fancy? Trends Immunol. *27*, 282–290. https://doi.org/10.1016/j.it.2006.04.004.

63. Conroy, M.J., Maher, S.G., Melo, A.M., Doyle, S.L., Foley, E., Reynolds, J.V., Long, A., and Lysaght, J. (2018). Identifying a Novel Role for Fractalkine (CX3CL1) in Memory CD8(+) T Cell Accumulation in the Omentum of Obesity-Associated Cancer Patients. Front. Immunol. *9*, 1867. https://doi.org/10.3389/fimmu.2018.01867.

64. Umehara, H., Tanaka, M., Sawaki, T., Jin, Z.X., Huang, C.R., Dong, L., Kawanami, T., Karasawa, H., Masaki, Y., Fukushima, T., et al. (2006). Fractalkine in rheumatoid arthritis and allied conditions. Mod. Rheumatol. *16*, 124–130. https://doi.org/10.1007/s10165-006-0471-9.

65. Barinov, A., Luo, L., Gasse, P., Meas-Yedid, V., Donnadieu, E., Arenzana-Seisdedos, F., and Vieira, P. (2017). Essential role of immobilized chemokine CXCL12 in the regulation of the humoral immune response. Proc. Natl. Acad. Sci. USA *114*, 2319–2324. https://doi.org/10.1073/pnas.1611958114.

66. Lang, R. (2005). Tuning of macrophage responses by Stat3-inducing cytokines: molecular mechanisms and consequences in infection. Immunobiology *210*, 63–76. https://doi.org/10.1016/j.imbio.2005.05.001.

67. Fu, Y., Wang, J., Zhou, B., Pajulas, A., Gao, H., Ramdas, B., Koh, B., Ulrich, B.J., Yang, S., Kapur, R., et al. (2022). An IL-9-pulmonary macrophage axis defines the allergic lung inflammatory environment. Sci. Immunol. *7*, eabi9768. https://doi.org/10.1126/sciimmunol.abi9768.

68. Mendez-Enriquez, E., and García-Zepeda, E.A. (2013). The multiple faces of CCL13 in immunity and inflammation. Inflammopharmacology *21*, 397–406. https://doi.org/10.1007/s10787-013-0177-5.

69. Sanchez-Martin, L., Estecha, A., Samaniego, R., Sanchez-Ramon, S., Vega, M.A., and Sanchez-Mateos, P. (2011). The chemokine CXCL12 regulates monocyte-macrophage differentiation and RUNX3 expression. Blood *117*, 88–97. https://doi.org/10.1182/blood-2009-12-258186.

70. Valentine, K.M., and Hoyer, K.K. (2019). CXCR5+ CD8 T Cells: Protective or Pathogenic? Front. Immunol. *10*, 1322. https://doi.org/10.3389/fimmu.2019.01322.

71. Valentine, K.M., Mullins, G.N., Davalos, O.A., Seow, L.W., and Hoyer, K.K. (2021). CD8 follicular T cells localize throughout the follicle during germinal center reactions and maintain cytolytic and helper properties. J. Autoimmun. *123*, 102690. https://doi.org/10.1016/j.jaut.2021.102690.

72. Leong, Y.A., Chen, Y., Ong, H.S., Wu, D., Man, K., Deleage, C., Minnich, M., Meckiff, B.J., Wei, Y., Hou, Z., et al. (2016). CXCR5(+) follicular cytotoxic T cells control viral infection in B cell follicles. Nat. Immunol. *17*, 1187–1196. https://doi.org/10.1038/ni.3543.

73. He, R., Hou, S., Liu, C., Zhang, A., Bai, Q., Han, M., Yang, Y., Wei, G., Shen, T., Yang, X., et al. (2016). Follicular CXCR5- expressing CD8(+) T cells curtail chronic viral infection. Nature *537*, 412–428. https://doi.org/10.1038/nature19317.

74. Velu, V., Mylvaganam, G., Ibegbu, C., and Amara, R.R. (2018). Tfh1 Cells in Germinal Centers During Chronic HIV/SIV Infection. Front. Immunol. *9*, 1272. https://doi.org/10.3389/fimmu.2018.01272.

75. Elzein, S.M., Zimmerer, J.M., Han, J.L., Ringwald, B.A., and Bumgardner, G.L. (2021). CXCR5(+)CD8(+) T cells: A Review of their Antibody Regulatory Functions and Clinical Correlations. J. Immunol. *206*, 2775–2783. https://doi.org/10.4049/jimmunol.2100082.

76. Groom, J.R., and Luster, A.D. (2011). CXCR3 in T cell function. Exp. Cell Res. *317*, 620–631. https://doi.org/10.1016/j.yexcr.2010.12.017.

77. Groom, J.R., and Luster, A.D. (2011). CXCR3 ligands: redundant, collaborative and antagonistic functions. Immunol. Cell Biol. *89*, 207–215. https://doi.org/10.1038/icb.2010.158.

78. Bangs, D.J., Tsitsiklis, A., Steier, Z., Chan, S.W., Kaminski, J., Streets, A., Yosef, N., and Robey, E.A. (2022). CXCR3 regulates stem and proliferative CD8+ T cells during chronic infection by promoting interactions with DCs in splenic bridging channels. Cell Rep. *38*, 110266. https://doi.org/10.1016/j.celrep.2021.110266.

79. Maurice, N.J., McElrath, M.J., Andersen-Nissen, E., Frahm, N., and Prlic, M. (2019). CXCR3 enables recruitment and site-specific bystander activation of memory CD8(+) T cells. Nat. Commun. *10*, 4987. https://doi.org/10.1038/s41467-019-12980-2.

80. Vanbervliet, B., Bendriss-Vermare, N., Massacrier, C., Homey, B., de Bouteiller, O., Brière, F., Trinchieri, G., and Caux, C. (2003). The inducible CXCR3 ligands control plasmacytoid dendritic cell responsiveness to the constitutive chemokine stromal cell-derived factor 1 (SDF-1)/CXCL12. J. Exp. Med. *198*, 823–830. https://doi.org/10.1084/jem.20020437.

81. Sallusto, F., Lenig, D., Förster, R., Lipp, M., and Lanzavecchia, A. (1999). Two subsets of memory T lymphocytes with distinct homing potentials and effector functions. Nature *401*, 708–712.

82. Turner, C.N., Mullins, G.N., and Hoyer, K.K. (2022). CXCR5(+)CD8 T cells: Potential immunotherapy targets or drivers of immune-mediated adverse events? Front. Med. *9*, 1034764. https://doi.org/10.3389/fmed.2022.1034764.

83. Breitfeld, D., Ohl, L., Kremmer, E., Ellwart, J., Sallusto, F., Lipp, M., and Förster, R. (2000). Follicular B helper T cells express CXC chemokine receptor 5, localize to B cell follicles, and support immunoglobulin production. J. Exp. Med. *192*, 1545–1552. https://doi.org/10.1084/jem.192.11.1545.

84. Petrovas, C., Ferrando-Martinez, S., Gerner, M.Y., Casazza, J.P., Pegu, A., Deleage, C., Cooper, A., Hataye, J., Andrews, S., Ambrozak, D., et al. (2017). Follicular CD8 T cells accumulate in HIV infection and can kill infected cells in vitro via bispecific antibodies. Sci. Transl. Med. *9*, eaag2285. https://doi.org/10.1126/scitranslmed.aag2285.

85. Trujillo-Ochoa, J.L., Kazemian, M., and Afzali, B. (2023). The role of transcription factors in shaping regulatory T cell identity. Nat. Rev. Immunol. *23*, 842–856. https://doi.org/10.1038/s41577-023-00893-7.

86. Hatzi, K., Nance, J.P., Kroenke, M.A., Bothwell, M., Haddad, E.K., Melnick, A., and Crotty, S. (2015). BCL6 orchestrates Tfh cell differentiation via multiple distinct mechanisms. J. Exp. Med. *212*, 539–553. https://doi.org/10.1084/jem.20141380.

87. Bergamaschi, C., Stravokefalou, V., Stellas, D., Karaliota, S., Felber, B.K., and Pavlakis, G.N. (2021). Heterodimeric IL-15 in Cancer Immunotherapy. Cancers *13*, 837. https://doi.org/10.3390/cancers13040837.

88. Havenar-Daughton, C., Carnathan, D.G., Torrents de la Peña, A., Pauthner, M., Briney, B., Reiss, S.M., Wood, J.S., Kaushik, K., van Gils, M.J., Rosales, S.L., et al. (2016). Direct Probing of Germinal Center Responses Reveals Immunological Features and Bottlenecks for Neutralizing Antibody Responses to HIV Env Trimer. Cell Rep. *17*, 2195–2209. https://doi.org/10.1016/j.celrep.2016.10.085.

89. Kalams, S.A., Felber, B.K., Mullins, J.I., Scott, H.M., Allen, M.A., de Rosa, S.C., Heptinstall, J., Tomaras, G.D., Hu, J., deCamp, A.C., et al. (2024). Focusing HIV-1 Gag T-cell responses to highly conserved regions by DNA vaccination in HVTN 119. JCI Insight *9*, e180819.

90. De Rosa, S.C., Edupuganti, S., Huang, Y., Han, X., Elizaga, M., Swann, E., Polakowski, L., Kalams, S.A., Keefer, M.C., Maenza, J., et al. (2020). Robust antibody and cellular responses induced by DNA-only vaccination for HIV. JCI Insight *5*, e137079. https://doi.org/10.1172/jci.insight.137079.

91. Chandrashekar, A., Yu, J., McMahan, K., Jacob-Dolan, C., Liu, J., He, X., Hope, D., Anioke, T., Barrett, J., Chung, B., et al. (2022). Vaccine protection against the SARS-CoV-2 Omicron variant in macaques. Cell *185*, 1549–1555.e11. https://doi.org/10.1016/j.cell.2022.03.024.

92. Valentin, A., Bergamaschi, C., Rosati, M., Angel, M., Burns, R., Agarwal, M., Gergen, J., Petsch, B., Oostvogels, L., Loeliger, E., et al. (2022). Comparative immunogenicity of an mRNA/LNP and a DNA vaccine targeting HIV gag conserved elements in macaques. Front. Immunol. *13*, 945706. https://doi.org/10.3389/fimmu.2022.945706.

93. Gary, E.N., Tursi, N.J., Warner, B., Parzych, E.M., Ali, A.R., Frase, D., Moffat, E., Embury-Hyatt, C., Smith, T.R.F., Broderick, K.E., et al. (2022). Mucosal chemokine adjuvant enhances synDNA vaccine-mediated responses to SARS-CoV-2 and provides heterologous protection in vivo. Cell Rep. Med. *3*, 100693. https://doi.org/10.1016/j.xcrm.2022.100693.

94. Bergamaschi, C., Pandit, H., Nagy, B.A., Stellas, D., Jensen, S.M., Bear, J., Cam, M., Valentin, A., Fox, B.A., Felber, B.K., and Pavlakis, G.N. (2020). Heterodimeric IL-15 delays tumor growth and promotes intratumoral CTL and dendritic cell accumulation by a cytokine network involving XCL1, IFN-gamma, CXCL9 and CXCL10. J. Immunother. Cancer *8*, e000599. https://doi.org/10.1136/jitc-2020-000599.

95. Velu, V., Mylvaganam, G.H., Gangadhara, S., Hong, J.J., Iyer, S.S., Gumber, S., Ibegbu, C.C., Villinger, F., and Amara, R.R. (2016). Induction of Th1-Biased T Follicular Helper (Tfh) Cells in Lymphoid Tissues during Chronic Simian Immunodeficiency Virus Infection Defines Functionally Distinct Germinal Center Tfh Cells. J. Immunol. *197*, 1832–1842. https://doi.org/10.4049/jimmunol.1600143.

96. Mylvaganam, G.H., Rios, D., Abdelaal, H.M., Iyer, S., Tharp, G., Mavigner, M., Hicks, S., Chahroudi, A., Ahmed, R., Bosinger, S.E., et al. (2017). Dynamics of SIV-specific CXCR5+ CD8 T cells during chronic SIV infection. Proc. Natl. Acad. Sci. USA *114*, 1976–1981. https://doi.org/10.1073/pnas.1621418114.

97. Perreau, M., Savoye, A.L., De Crignis, E., Corpataux, J.M., Cubas, R., Haddad, E.K., De Leval, L., Graziosi, C., and Pantaleo, G. (2013). Follicular helper T cells serve as the major CD4 T cell compartment for HIV-1 infection, replication, and production. J. Exp. Med. *210*, 143–156. https://doi.org/10.1084/jem.20121932.

98. Pantaleo, G., Graziosi, C., Butini, L., Pizzo, P.A., Schnittman, S.M., Kotler, D.P., and Fauci, A.S. (1991). Lymphoid organs function as major reservoirs for human immunodeficiency virus. Proc. Natl. Acad. Sci. USA *88*, 9838–9842.

99. Collins, D.R., Gaiha, G.D., and Walker, B.D. (2020). CD8(+) T cells in HIV control, cure and prevention. Nat. Rev. Immunol. *20*, 471–482. https://doi.org/10.1038/s41577-020-0274-9.

100. Buckley, M., Arainga, M., Maiorino, L., Pires, I.S., Kim, B.J., Michaels, K.K., Dye, J., Qureshi, K., Zhang, Y., Mak, H., et al. (2024). Visualizing lipid nanoparticle trafficking for mRNA vaccine delivery in non-human primates. Mol Ther. *33*, 1105–1117. https://doi.org/10.1101/2024.06.21.600088.

101. Smith, A.R., Rizvi, F., Everton, E., Adeagbo, A., Wu, S., Tam, Y., Muramatsu, H., Pardi, N., Weissman, D., and Gouon-Evans, V. (2024). Transient growth factor expression via mRNA in lipid nanoparticles promotes hepatocyte cell therapy to treat murine liver diseases. Nat. Commun. *15*, 5010.

102. Kapellos, T.S., Bonaguro, L., Gemünd, I., Reusch, N., Saglam, A., Hinkley, E.R., and Schultze, J.L. (2019). Human Monocyte Subsets and Phenotypes in Major Chronic Inflammatory Diseases. Front. Immunol. *10*, 2035. https://doi.org/10.3389/fimmu.2019.02035.

103. Lee, J., Tam, H., Adler, L., Ilstad-Minnihan, A., Macaubas, C., and Mellins, E.D. (2017). The MHC class II antigen presentation pathway in human monocytes differs by subset and is regulated by cytokines. PLoS One *12*, e0183594. https://doi.org/10.1371/journal.pone.0183594.

104. Embgenbroich, M., and Burgdorf, S. (2018). Current Concepts of Antigen Cross-Presentation. Front. Immunol. *9*, 1643. https://doi.org/10.3389/fimmu.2018.01643.

105. Chancellor, A., Gadola, S.D., and Mansour, S. (2018). The versatility of the CD1 lipid antigen presentation pathway. Immunology *154*, 196–203. https://doi.org/10.1111/imm.12912.

106. Arunachalam, P.S., Lai, L., Samaha, H., Feng, Y., Hu, M., Hui, H.S.Y., Wali, B., Ellis, M., Davis-Gardner, M.E., Huerta, C., et al. (2023). Durability of immune responses to mRNA booster vaccination against COVID-19. J. Clin. Investig. *133*, e167955. https://doi.org/10.1172/JCI167955.

107. Thomopoulos, T.P., Rosati, M., Terpos, E., Stellas, D., Hu, X., Karaliota, S., Bouchla, A., Katagas, I., Antoniadou, A., Mentis, A., et al. (2021). Kinetics of Nucleocapsid, Spike and Neutralizing Antibodies, and Viral Load in Patients with Severe COVID-19 Treated with Convalescent Plasma. Viruses *13*, 1844. https://doi.org/10.3390/v13091844.

108. Terpos, E., Stellas, D., Rosati, M., Sergentanis, T.N., Hu, X., Politou, M., Pappa, V., Ntanasis-Stathopoulos, I., Karaliota, S., Bear, J., et al. (2021). SARS-CoV-2 Antibody Kinetics Eight Months from COVID-19 Onset: Persistence of Spike Antibodies but Loss of Neutralizing Antibodies in 24% of Convalescent Plasma Donors. Eur. J. Intern. Med. *89*, 87–96. https://doi.org/10.1016/j.ejim.2021.05.010.

109. Rosati, M., Terpos, E., Ntanasis-Stathopoulos, I., Agarwal, M., Bear, J., Burns, R., Hu, X., Korompoki, E., Donohue, D., Venzon, D.J., et al. (2021). Sequential Analysis of Binding and Neutralizing Antibody in COVID-19 Convalescent Patients at 14 months after SARS-CoV-2 infection. Front. Immunol. *12*, 793953. https://doi.org/10.3389/fimmu.2021.793953.

110. Sette, A., Sidney, J., and Crotty, S. (2023). T Cell Responses to SARS-CoV-2. Annu. Rev. Immunol. *41*, 343–373. https://doi.org/10.1146/annurev-immunol-101721-061120.

111. Devasundaram, S., Terpos, E., Rosati, M., Ntanasis-Stathopoulos, I., Bear, J., Burns, R., Skourti, S., Malandrakis, P., Trougakos, I.P., Dimopoulos, M.A., et al. (2023). XBB.1.5 neutralizing antibodies upon bivalent COVID-19 vaccination are similar to XBB but lower than BQ.1.1. Am. J. Hematol. *98*, E123–E126. https://doi.org/10.1002/ajh.26887.

112. Bankhead, P., Loughrey, M.B., Fernández, J.A., Dombrowski, Y., McArt, D.G., Dunne, P.D., McQuaid, S., Gray, R.T., Murray, L.J., Coleman, H.G., et al. (2017). QuPath: Open source software for digital pathology image analysis. Sci. Rep. *7*, 16878. https://doi.org/10.1038/s41598-017-17204-5.

113. Halekoh, U., Højsgaard, S., and Yan, J. (2006). The R Package geepack for Generalized Estimating Equations. J. Stat. Softw. *15*, 1–11.

114. Kolde, R. (2019). Pheatmap: pretty heatmaps. R package version *1*, 726.

115. Wei, T., Simko, V., Levy, M., Xie, Y., Jin, Y., and Zemla, J. (2017). Package 'corrplot'. Statistician *56*, e24. https://github.com/taiyun/corrplot.

116. Kuznetsova, A., Brockhoff, P.B., and Christensen, R.H.B. (2017). lmerTest Package: Tests in Linear Mixed Effects Models. J. Stat. Softw. *82*, 1–26. https://doi.org/10.18637/jss.v082.i13.

117. Shah, N.A., Bhatt, L.K., Patel, R.J., Patel, T.M., Patel, N.V., Trivedi, H.G., Patel, N.R., Patel, J.H., Patel, S.D., Sundar, R.S., and Jain, M.R. (2022). Hematological and biochemical reference intervals of wild-caught and in-house adult Indian rhesus macaques (Macaca mulatta). Lab. Anim. Res. *38*, 33. https://doi.org/10.1186/s42826-022-00143-2.

118. Schmidt, F., Weisblum, Y., Muecksch, F., Hoffmann, H.H., Michailidis, E., Lorenzi, J.C.C., Mendoza, P., Rutkowska, M., Bednarski, E., Gaebler, C., et al. (2020). Measuring SARS-CoV-2 neutralizing antibody activity using pseudotyped and chimeric viruses. J. Exp. Med. *217*, e20201181. https://doi.org/10.1084/jem.20201181.

119. Strongin, Z., Raymond Marchand, L., Deleage, C., Pampena, M.B., Cardenas, M.A., Beusch, C.M., Hoang, T.N., Urban, E.A., Gourves, M., Nguyen, K., et al. (2024). Distinct SIV-specific CD8(+) T cells in the lymph node exhibit simultaneous effector and stem-like profiles and are associated with limited SIV persistence. Nat. Immunol. *25*, 1245–1256. https://doi.org/10.1038/s41590-024-01875-0.

## STAR★METHODS

### KEY RESOURCES TABLE

| REAGENT or RESOURCE | SOURCE | IDENTIFIER |
|---|---|---|
| Antibodies | | |
| Mouse anti-human CD3, Clone SP34-2, APC-Cy7 | BD Biosciences | Cat#557757; RRID:AB_396863 |
| Mouse anti-human CD3, Clone SP34-2, PE | BD Biosciences | Cat#560811; RRID:AB_2033927 |
| Mouse anti-human CD4, Clone L200, V450 | BD Biosciences | Cat#562402; RRID:AB_11153863 |
| Mouse anti-human CD4, Clone L200, BUV395 | BD Biosciences | Cat#564107; RRID:AB_2738596 |
| Mouse anti-human CD8a, Clone RPA-T8, Brilliant Violet 650 | BioLegend | Cat#301042; RRID:AB_2563505 |
| Mouse anti-human CD8, Clone RPA-T8, BUV496 | BD Biosciences | Cat#612942; RRID:AB_2870223 |
| Mouse anti-human CD28, Clone RPA-T8, PerCP/Cyanine5.5 | BioLegend | Cat#302922; RRID:AB_2073718 |
| Mouse anti-human CD28, Clone V-CD28.05, Brilliant Violet 785 | BioLegend | Cat#302950; RRID:AB_2632607 |
| Mouse anti-human CD95, Clone DX2, FITC | BD Biosciences | Cat#556640; RRID:AB_396506 |
| Mouse anti-human CD95, BV480 | BD Biosciences | Cat#746675; RRID:AB_2743947 |
| Mouse anti-human CD95, PE CF594 | BD Biosciences | Cat#562395; RRID:AB_11153666 |
| Mouse anti-human CD107a (LAMP-1) Monoclonal Antibody (eBioH4A3), PE, eBioscience | Thermo Fisher Scientific | Cat#12-1079-42; RRID:AB_10853326 |
| Mouse anti-human CD107a (LAMP-1) Monoclonal Antibody (eBioH4A3), eFluor 660, eBioscience | Thermo Fisher Scientific | Cat#50-1079-42; RRID:AB_11220283 |
| Mouse anti-human Granzyme B Monoclonal Antibody (GB12), APC | Thermo Fisher Scientific | Cat#MHGB05; RRID:AB_1500190 |
| Mouse anti-human Granzyme B, Clone GB11, BV421 | BD Biosciences | Cat#563389; RRID:AB_2738175 |
| Mouse anti-human Granzyme B, Clone GB11, Alexa Fluor 700 | BD Biosciences | Cat#560213; RRID:AB_1645453 |
| Mouse anti-human Ki-67, Clone B56 Alexa Fluor® 700 | BD Biosciences | Cat#561277; RRID:AB_10611571 |
| Mouse anti-human Ki-67, Clone B56, BV711 | BD Biosciences | Cat#563755; RRID:AB_2738406 |
| Mouse anti-human IFN-g, Clone B27, PE-Cy7 | BD Biosciences | Cat#557643; RRID:AB_396760 |
| LIVE/DEAD™ Fixable Blue Dead Cell Stain Kit, for UV excitation | Thermo Fisher Scientific | Cat#L34962 |
| Rat anti-human (CD197) CCR7, Clone 3D12, BUV737 | BD Biosciences | Cat#741786; RRID:AB_2871135 |
| Rat anti-mouse CD197 (CCR7), Clone 4B12, BUV737 | BD Biosciences | Cat#741892; RRID:AB_2871211 |
| Mouse anti-human CD197 (CCR7), Clone 2-L1-A, BUV661 | BD Biosciences | Cat#749824; RRID:AB_2874072 |
| Mouse anti-human EOMES Monoclonal Antibody (WD1928), FITC, eBioscience | Thermo Fisher Scientific | Cat#11-4877-42; RRID:AB_2572499 |
| Mouse anti-human T-bet monoclonal antibody (eBio4B10 (4B10), PE-Cyanine5, eBioscience | Thermo Fisher Scientific | Cat#15-5825-82; RRID:AB_2815071 |
| Mouse anti-human TNF, Clone Mab11, Alexa Fluor® 700 | BD Biosciences | Cat#557996; RRID-AB_396978 |
| Mouse anti-human CD20, BV605 | BD Biosciences | Cat#747736; RRID:AB_2872209 |
| Mouse anti-human CD20, Clone 2H7, PE | BD Biosciences | Cat#555623; RRID:AB_395989 |
| Mouse anti-human TCR gamma/delta monoclonal antibody (5A6.E9), FITC | Thermo Fisher Scientific | Cat#TCR2061; RRID:AB_223620 |
| Mouse anti-human CD159a (NKG2A)-APC, Z199 | Beckman Coulter | Cat#A60797; RRID:AB_10643105 |
| Mouse anti-human CD159a (NKG2A)-PE, Z199 | Beckman Coulter | Cat#IM3291U; RRID:AB_10643228 |
| Mouse anti-human CD25, Clone M-A251, BUV805 | BD Biosciences | Cat#742011; RRID:AB_2871309 |
| Mouse anti-human CD196 (CCR6), Clone 11A9, BV650 | BD Biosciences | Cat#563922; RRID:AB_2738488 |
| Mouse anti-human CD127 (IL-7Rα), PerCP/Cyanine5.5 | BioLegend | Cat#351322; RRID:AB_10897104 |
| Mouse anti-human CD183, Clone 1C6/CXCR3, BUV563 | BD Biosciences | Cat#741406; RRID:AB_2870896 |
| Mouse anti-human CD185 (CXCR5) Monoclonal Antibody (MU5UBEE), PE, e-Bioscience | Thermo Fisher Scientific | Cat#12-9185-42; RRID:AB_11219877 |
| Mouse anti-human PE-Cyanine7 anti-human CD279 (PD-1) Antibody, clone EH12.2H7 | BioLegend | Cat#329918; RRID:AB_2159324 |

(*Continued on next page*)

*Continued*

| REAGENT or RESOURCE | SOURCE | IDENTIFIER |
|---|---|---|
| Mouse anti-human HLA-DR, Clone G46-6, BUV661 | BD Biosciences | Cat#612980; RRID:AB_2870252 |
| Mouse anti-human Bcl-2, PE-CF594 | BD Biosciences | Cat#563601; RRID:AB_2738307 |
| Mouse anti-human Bcl-6, BV421 | BD Biosciences | Cat#563363; RRID:AB_2738159 |
| Mouse anti-human CD11c, Clone 3.9, PE/Cyanine5 | BioLegend | Cat#301610; RRID:AB_493578 |
| Chicken anti-human SynCAM (TSLC1/CADM1) mAb-Alexa Fluor 647, Clone 3E1 | MBL | Cat#CM004-A64; RRID:AB 3107120 |
| Mouse anti-human CD1c, Clone L161, Alexa Fluor® 700 | BioLegend | Cat#331530; RRID:AB_2563657 |
| Rat anti-mouse CD11b, Clone M1/70, APC-Cy7 Tested in Development: Human | BD Biosciences | Cat#557657; RRID:AB_396772 |
| Rat anti-human Clec9A (CD370), Clone 3A4/Clec9A, BV421 | BD Biosciences | Cat#564266; RRID:AB_2738716 |
| Mouse anti-human CD16, Clone 3G8, BV480 | BD Biosciences | Cat#566108; RRID:AB_2739510 |
| Mouse anti-human CD123, Clone 7G3, BV786 | BD Biosciences | Cat#564196; RRID:AB_2738662 |
| Mouse anti-human CD14, Clone M5E2, BUV737 | BD Biosciences | Cat#612764; RRID:AB_2870095 |
| Mouse anti-human IRF8 monoclonal antibody (V3GYWCH), PerCP-eFluor 710, eBioscience | Thermo Fisher Scientific | Cat#46-9852-82; RRID: AB_2573904 |
| Mouse anti-human IRF4 Monoclonal Antibody (3E4), PE-eFluor™ 610, eBioscience | Thermo Fisher Scientific | Cat#61-9858-82; RRID:AB_2637108 |
| Mouse anti-human CD27, Clone M-T271, BV421 | BD Biosciences | Cat#562513; RRID:AB_11153497 |
| CD278 (ICOS) Armenian Hamster, PE-CF594, Clone: C398.4A | BD Biosciences | Cat#565888; RRID:AB_2869727 |
| Mouse anti-human CD134, Clone L106, BV480 | BD Biosciences | Cat#746511; RRID:AB_2743808 |
| Mouse anti-human CD137 (4-1BB), Brilliant Violet 711 | BioLegend | Cat#309832; RRID:AB_2650991 |
| Mouse anti-human HLA-DR, Clone G46-6, BUV737 | BD Biosciences | Cat#568351; RRID:AB_2691827 |
| **Biological samples** | | |
| Peripheral blood mononuclear cells (PBMC) | This paper | N/A |
| Lymph node mononuclear cells (LNMC) | This paper | N/A |
| Human serum | Sigma | Cat#H4522 |
| Macaque plasma/serum | This paper | N/A |
| **Chemicals, peptides, and recombinant proteins** | | |
| Ficoll-hypaque | GE Healthcare | Cat#17-1440-03 |
| Ionomycin | eBiosciences | Cat#00-4970 |
| WA.1 Spike Receptor Binding Domain (RBD) protein | in-house | N/A |
| BA.1 Spike-RBD protein | in-house | N/A |
| SARS-CoV-2 Spike Peptide Pool | Pep-Mix SARS-CoV-2 JPT or Biosynthesis | |
| **Critical commercial assays** | | |
| U-PLEX NHP Biomarker Assay kit | Meso Scale Diagnostics LLC | Cat#K15082K-2 |
| V-PLEX Human IL-21 Kit | Meso Scale Diagnostics LLC | Cat#K151WUD-1 |
| ELISA, human CXCL13 | Invitrogen | Cat#EHCXCL13 |
| ELISA, macaque IL-27 | MyBioSource | Cat#MBS015294 |
| FoxP3 staining kit | eBioscience | Cat#00-55523-00 |
| **Deposited data** | | |
| Raw FACS data | This paper | https://github.com/NCI-VB/felber_LION_macaque/blob/main/input_data/list_of_RAW_datasets.xlsx |
| Cell population frequencies and raw MSD data | This paper | https://github.com/NCI-VB/felber_LION_macaque/blob/main/input_data/list_of_RAW_datasets.xlsx |
| **Experimental models: Organisms/strains** | | |
| *M. mulatta*-Indian Rhesus macaques | Bioqual | N/A |

(*Continued on next page*)

*Continued*

| REAGENT or RESOURCE | SOURCE | IDENTIFIER |
|---|---|---|
| Recombinant DNA | | |
| WA1 Spike (2P-stabilized 1273-AA) | Rosati et al.[32] | plasmid code C57 |
| BA.1 (B.1.1.529) (2P-stabilized 1273-AA) | This paper | plasmid code C121 |
| BA.4/5 (2P-stabilized 1273-AA) | This paper | plasmid code C123 |
| WA1 (D614G, 1254-AA) Spike | Devasundaram et al.[111] | plasmid code C77 |
| BA.1(D614G, 1254-AA) Spike | Devasundaram et al.[111] | plasmid code C120 |
| BA4/5 (D614G, R683G 1254-AA) Spike | Devasundaram et al.[111] | plasmid code C123 |
| BQ1.1 (D614G, 1254-AA) Spike | Devasundaram et al.[111] | plasmid code C124 |
| XBB1.5 (D614G, 1254-AA) Spike | Devasundaram et al.[111] | plasmid code C127 |
| Software and algorithms | | |
| Original code | This paper | https://github.com/NCI-VB/felber_LION_macaque |
| GraphPad prism v. 10.4.1 for MacOS X | GraphPad Software, Inc. | |
| FlowJo | Tree Star, Inc. | |
| QuPath | Bankhead et al.[112] | |
| geepack R package (v1.3.10) | Halekoh et al.[113] | https://cran.r-project.org/web/packages/geepack/index.html |
| pheatmap R package (v1.0.12) | Kolde et al.[114] | https://cran.r-project.org/web/packages/pheatmap/index.html |
| corrplot R Package (v0.92) | Wei and Simko[115] | https://cran.r-project.org/web/packages/corrplot/index.html |
| lmerTest r package (v3.1.3) | Kuznetsova et al.[116] | https://cran.r-project.org/web/packages/lmerTest/index.html |
| Other | | |
| Pheno-Cycler Fusion Technology | Akoya Biosciences | N/A |
| Symphony and Fortessa Flow Cytometers | BD Biosciences | N/A |

## EXPERIMENTAL MODEL AND STUDY PARTICIPANT DETAILS

### Non human primates

Studies in Indian rhesus macaques were conducted in compliance with all relevant local, state, and federal regulations and were approved by the BIOQUAL Institutional Animal Care and Use Committee (IACUC) (Approval #21-032P). All macaques were male and between 5 and 11 years old as detailed in Table S1.

## METHOD DETAILS

### Vaccination

The animals (Table S1) were vaccinated via the intramuscular (IM) route as outlined in Figure 1B (Study 1, wk 0, 4, 38, 88) or Figure 1D (Study 2, wk 0, 4). CBC/Chem was monitored in study 1 upon vaccination 4 and compared to ranges reported for wild-caught macaques.[117]

The vaccine regimens comprised Spike DNA/LION (Study 1, group 1 and Study 2) and naked Spike DNA (DNA/IM; Study 1, group 2). Previously reported data[32] from macaques vaccinated by electroporation (EP) of WA.1 Spike DNA alone or DNA+Protein co-immunizations were included. The vaccine comprised DNAs expressing the following 2P-stabilized 1273-AA Spike proteins including wildtype WA1 Spike[32]; Omicron BA.1 (B.1.1.529) (plasmid code C121); Omicron BA.4/5 (plasmid code C123) in study 1 and Omicron BA.1 (B.1.1.529) in study 2. The Spike genes were inserted between the human CMV promoter and the BGH polyadenylation signal of the expression vector pCMV.kan.[32] The vaccine dose was 2 mg and included 0.1 mg rmIL-12 DNA (plasmid code AG157) in vaccinations V1-V3.

LION nanocarrier composition is detailed elsewhere[27,28] and the oil phase contains squalene, DOTAP, SPAN 60, Tween 80. The vaccine (2 mL) was administered in 2 × 0.5 mL, injected 2 cm apart, to the inner left and right thigh, respectively, for vaccinations 1–3. For vaccination 4, the vaccine was administered in 4 × 0.5 mL in inner left and right thighs and in left and right arms.

Animals (group 1; $n = 5$) received 4 DNA/LION vaccinations and were compared to animals (group 2; $n = 3$) receiving 2 vaccinations with naked DNA as prime, subsequently received 2 DNA/LION booster vaccinations. Naked DNA was injected in 2 × 0.5 mL, injected

2 cm apart, to the inner left and right thigh, respectively. Blood was collected after each vaccination as indicated and lymph nodes were collected after vaccination 4 [D1 (inguinal; $n = 8$), D3 (axillary; $n = 4$), D4 (axillary; $n = 4$)), D8 (axillary, $n = 8$), D22 (inguinal; $n = 8$)]. Samples from D3 and D4 were combined (D3/4). Tissues collected at D3/4 and D8 represent draining LN. In study 2, animals ($n = 5$) received 2 DNA/LION vaccinations using 2 mg of stabilized Omicron BA.1 (B.1.1.529) DNA.

### Cytokine/chemokine analysis

Samples were collected at the day of vaccination (D1), 4 h later and at D2, D4, and D8 after each vaccination. For vaccination 4 (V4), the 4 hr-sample was not collected, and animals were analyzed in addition at D15 and D22. Serum cytokine/chemokine levels (pg/mL), monitoring 63 analytes (Table S2), were measured with the: U-PLEX NHP Biomarker Assay kit (K15082K-2, Meso Scale Diagnostics LLC, MD, USA); IL-21 was measured by V-PLEX Human IL-21 Kit (K151WUD-1, Meso Scale Diagnostics LLC, MD, USA); CXCL13 was measured by commercial ELISA (Invitrogen cat# EHCXCL13) at 1:2 dilution; macaque IL-27 was measured by ELISA using undiluted samples (MyBioSource, cat# MBS015294). Biomarker levels falling below the detection limit/standard range were removed if absent in more than 50% of the samples or adjusted to 50% of the lowest standard point or detection limits. The cytokine analysis following vaccination 1 and 2 included measurements from 5 additional macaques which received the BA.1 Spike DNA/LION vaccine using the same dose and schedule (study 2).

### SARS-CoV-2 antibody measurements

Binding antibody responses were measured by an in-house ELISA to wildtype Wuhan (WA1) or BA.1 Spike-RBD as detailed elsewhere.[32,109,111] The ELISA measurements of the Spike antibody titers of the historical samples (two weeks after vaccination) were performed together with the eight animals enrolled in this study. Ab levels were measured using eight 4-fold serial plasma dilutions starting at 1:50 and endpoint titers were determined using lastX feature using GraphPad prism area-under-the curve program. Pseudotype neutralization was performed using a $HIV_{NL}\Delta$Env-Nanoluc assay carrying the 1254-AA WA1 (D614G), BA.1, BA.4/5, BQ1.1 and XBB1.5 Spike proteins.[118] The highest serum concentration analyzed was a 1:40 dilution and 8 4-fold serial dilutions were tested. Two days later, the luciferase levels were measured in the cell extracts as ID50 (50% Inhibitory Dose) calculated using GraphPad Prism version 10.4.1 for MacOS X (GraphPad Software, Inc, La Jolla, CA).

### Isolation of PBMC and preparation of single-cell suspensions from LNs

PBMCs were isolated using Ficoll-Hypaque (GE Healthcare) based on the manufacturer's instructions. Lymph nodes were transported on wet ice in complete RPMI medium within 2h from surgery. To isolate mononuclear cells, lymph nodes tissues were crushed on a 100 μm strainer (BD) using the plunger of a 3 mL sterile syringe. Cells were washed in PBS, counted, and cryopreserved.

### Antigen-specific T cell responses in blood

Antigen-specific T cells were measured by flow cytometry[32] in Ficoll-Paque Plus (GE-17-1440-03, GE Healthcare, Sweden)-purified PBMC. Cells were cultured in 96-well plates for 12 h in the presence of SARS-CoV-2 Spike peptide pools (Pep-Mix SARS-CoV-2 JPT or Biosynthesis), at a final concentration of 1 μg/mL for each individual peptide. Incubation in medium without peptide stimulation or in the presence of a cell stimulation cocktail containing PMA and ionomycin (Cat#: 00–4970, eBioscience, San Diego, CA), were used as negative and positive controls, respectively. The protein transport inhibitor monensin (GolgiStop, Cat#51-2092KZ, BD Biosciences, San Jose, CA) was added to the wells to prevent cytokine secretion at 60 min after adding the peptides. A 9- color (Figure 2C) and a 14-color (Figures 2D–2G) antibody panel was used to measure Spike-specific responses as detailed in Tables S3 and S4. Samples were acquired on a Fortessa flow cytometer (BD Biosciences, San Jose, CA), and the data were analyzed using FlowJo software (Tree Star, Inc., Ashland, OR). The T cell analysis of the historical samples used the same protocol, the same peptide pool and antibody panel and the same operator, ensuring consistency and reliability in the comparisons. Samples were considered positive if the frequency of cytokine-positive T cells was 2-fold higher than the unstimulated medium-only control and exceeded 0.05 after subtracting the value of the medium control. Cell subset analysis was performed as outlined in Table S5.

### Immune cell phenotyping and flow cytometry

Manual gating analysis: Frozen PBMC and LNMC were thawed, washed, and resuspend in culture medium. At least 1 million cells from each sample were washed with PBS and then resuspended in LIVE/DEAD Fixable Dead Cell Stain mixture (Thermo Fischer cat# L34962). Following a 30-min incubation at 4°C, the cells were washed with PBS supplemented with 0.2% heat-inactivated human serum (Sigma) and 2mM EDTA (Thermo Fischer cat# 15575020) and incubated with different panels (Figures S9 and S10) of fluorophore-labelled monoclonal antibodies for 20 min at room temperature as listed in Tables S6 and S7. After cell surface staining, the cells were washed once and fixed/permeabilized using the FoxP3 staining kit (eBioscience cat# 00-5523-00). After 30 min incubation at 4°C, the cells were washed with FoxP3 washing buffer and intracellularly stained with cocktails of fluorophore-labelled monoclonal antibodies targeting intracellular antigens (Table S8) for 20 min. The cells were washed and resuspended in PBS for flow cytometry analysis. The samples were acquired in a Symphony flow cytometer (BD Biosciences, San Jose, CA), and the data were analyzed using the FlowJo software platform (Tree Star, Inc., Ashland, OR). No significant differences were found in lymph node and blood samples collected at day 3 and 4 (4 animals each) and data were combined for the analysis, labeled D3/4. All other timepoints comprised of 8 animals. Mean Fluorescent Intensity (MFI) of Eomes, T-bet, GzmB and Ki67 expression by Spike-stimulated CD8

T cells in blood was assessed by concatenating CD8 T cells (3000 cells/timepoint/Animal ($n$ = 8)). The concatenated CD8 cells were first gated as $T_{CM}$ or $T_{EM}$ based on CD95 and CD28 markers and then gated on CD107a, IFN-$\gamma$ and TNF-$\alpha$. Samples at V4, V4w2 and V4w3 ($n$ = 8/timepoint), were identified and shown simultaneously in a common histogram plot allowing cross-comparison (Figure 2G).

Unsupervised analysis: Live cell subsets were manually gated following exclusion of dead cells and doublets. Equivalent number of cells per each animal were concatenated together and used for unsupervised T-distributed stochastic neighbor embedding (t-SNE) analysis based on forward scatter, side scatter and selected phenotypic markers. The common t-SNE map was applied subsequently on respective samples to allow cross-comparison between timepoints and/or compartments. t-SNE visualisation of general lineage population in LN and blood was performed using 160,000 total live cells at D1 (10,000/timepoint/compartment from all 8 animals) based on the markers CD20, CD3 and HLA-DR (Figure 4B). For analysis of proliferating LNMC subsets, a total of 32,000 $Ki67^+$ lymphocytes (myeloid cells being excluded based on side and forward scatter), were used to generate t-SNE map (1,000 cells/timepoint from all 8 animals) based on the markers CD20, CD3, CD4, CD8, CCR6, Bcl-2, Bcl-6, CXCR3, CXCR5 and PD-1 (Figure 6A).

### AIM assay

Live-frozen LNMC were thawed, washed, and rested at a concentration of $10x10^6$ cells/ml in AIM-V medium (CTS AIM-V Medium, Gibco, ref. 0870112-DK) for 3 hrs at 37°C. Subsequently, $1x10^6$ cells/well were seeded in a 96-well U-bottom plate and incubated for 24hrs in presence of a mixture containing SARS-CoV-2 Spike peptide pool (297 peptides; 15-mer, 11AA overlap, each at 1 μg/mL; COVID-19 S, Biosynthesis) and SARS-CoV-2 Trimeric Spike protein (VRC-SARS-CoV-2 S-2P(15–1208)-3C-His8-Strep2x2; at 1 μg/mL), or medium plus DMSO (0.2%). The plate was centrifuged, and supernatants were harvested for MSD analysis and the cells were stained with a panel of surface antibodies as detailed in Table S8.

### High-plex *in situ* spatial phenotyping analysis

Formalin-fixed paraffin-embedded LN, collected at D3/4, 8 and 22 ($n$ = 7) post $4^{th}$ vaccination, and 3 LN collected from naive unvaccinated macaques from a previous study were stained using the Pheno-Cycler Fusion technology, allowing the detection of several proteins on same tissue section. We designed and validated a panel of 21-markers to analyze the effects of DNA/LION vaccination in LN.[119] Immunostaining for use with the Phenocycler-Fusion was performed following the Akoya reference manual. Oligonucleotide-barcoded antibodies were conjugated and validated on gel and on control tissues and cell lines. Some antibody working dilutions had to be adjusted like: CD3 (Cat 4550125), CD68 (Cat 4550113) stock antibodies were diluted 1:500 and CD20 (Cat 415001S), DC-SIGN (ab21SSS3 Abcam), HLA-DR (cat 455011S), Ki67 (cat 4250019) stock antibodies were diluted 1:1000 in universal antibody dilution buffer (Sigma, U3635), all other antibodies were used at 1:200. The antibody cocktail was prepared by combining antibody blocking solution (Staining buffer with N blocker, J blocker, S blocker, G blocker – Akoya Biosciences, 7000017) with each barcoded antibody diluted at its optimal dilution in blocking solution. Slides were incubated in the antibody cocktail over night at 4°C and subsequently washed 2 × 2 min in Staining buffer, fixed in 1.6% paraformaldehyde (32% PFA- Electron Microscopy Sciences, 15714-S in Storage buffer- Akoya Biosciences, 7000017) for 10 min at RT, rinsed 3x in 1x Phosphate Buffered Saline (PBS), post-fixed in ice-cold Methanol for 5 min, and rinsed 3x in 1xPBS. The slides were incubated in a final fixation solution (Akoya Biosciences, 7000017) for 20 min at RT, rinsed 3x in 1xPBS, and transferred to PhenoCycler buffer (Akoya Biosciences, 7000019) for 10 min. Flow cells (Akoya Biosciences, 240205) were adhered to slides for 30 s, and returned to PhenoCycler buffer for 10 min. Slides were loaded onto the PhenoCycler instrument for image acquisition setup following the instrument acquisition software and manufacturers protocol. 96-well fluorescent reporter plates (Akoya Biosciences, 7000006) for cyclic barcoded antibody reveal were prepared according to the Akoya manual. Three fluorescent reporters (Akoya Biosciences, RX001-RX500) corresponding to each DNA-barcoded antibody were added to each well containing a reporter master mix (PhenoCycler buffer, assay reagent (Akoya Biosciences, 7000002), and nuclear stain (Akoya Biosciences, 7000003). Panels contained two blank cycles of only reporter master mix without fluorescent reporters were used for background subtraction. Cyclic antibody reveal by 8 reporter cycles (21 antibody targets). All image visualization, processing, and analysis was performed using nuclei segmentation and marker expression for cell detection and quantified in QuPath[112] using specific threshold for each marker. Each tissue area was selected by hand using region of interest including all B-cell follicle and covering the majority of the T cell zone.

## QUANTIFICATION AND STATISTICAL ANALYSIS

Curated biomarkers and manual-gated cell population frequencies were compared to their baseline (D1) or other timepoint values to assess changes with time by fitting generalized estimating equations (GEE) with animal as a random effect, implemented by the geeglm function in the geepack package (v1.3.10).[113] Heatmaps were generated using the heatmap R package (v1.0.12).[114] Spearman associations were calculated among biomarkers or between cell populations and biomarkers or between cell populations and antibody titers, and correlation plots were generated with the corrplot R package (v0.92).[115] IHC data with multiple instances per sample were compared using linear mixed effect models, as implemented by the lmerTest r package (v3.1.1).[116] $p$-values are defined as $\leq$ 0.05, *; $\leq$0.01, **; $\leq$0.001, ***; $\leq$0.0001,****. Full code can be found at https://github.com/NCI-VB/felber_LION_macaque.